Chem Soc Rev

The Bridge Between Cationic and Anionic Redox in Rechargeable Lithium Battery

Journal:	*Chemical Society Reviews*
Manuscript ID	CS-SYN-05-2018-000426.R2
Article Type:	Review Article
Date Submitted by the Author:	11-Jan-2020
Complete List of Authors:	Zhong, Cheng; Tianjin University, School of Materials Science and Engineering Li, Matthew; Argonne National Laboratory, Chemical Science and Engineering Division Liu, Tongchao; Argonne National Laboratory, Chemical Science and Engineering Division Bi, Xuanxuan; Argonne National Laboratory, Chemical Science and Engineering Division Chen, Zhongwei; University of Waterloo, Chemical Engineering Amine, Khalil; Argonne National Laboratory, Lu, Jun; Argonne National Laboratory, Chemical Science and Engineering Division

ARTICLE

Cationic and Anionic Redox in Lithium-ion based Batteries

Matthew Li[a,b], Tongchao Liu[a], Xuanxuan Bi[a], Zhongwei Chen[b], Khalil Amine[a,d,e], Cheng Zhong[c*], Jun Lu[a*]

Received 00th January 20xx,
Accepted 00th January 20xx

DOI: 10.1039/x0xx00000x

Lithium-ion batteries have proven itself to be indispensable among modern day society. Demands stemming from consumer electronics and renewable energy systems have pushed researchers to strive for new electrochemical technologies. To this end, the advent of anionic redox that is, the sequential or simultaneous redox of the cation and anion in a transition metal oxide based cathode for a Li-ion battery has garnered much attention due to their enhanced specific capacities. Unfortunately, their higher energy densities are plagued with problems associated with the irreversibility of anionic redox. Much effort has been placed to find a suitable composition of transition metal oxide, with some groups identifying the underlying features and relationship for anion redox and cationic redox to occur reversibly. Accordingly, it is timely to review anionic redox in terms of: what is anionic redox with emphasis on mechanism and the evidence underlying their discovery and validation. To follow will be a section defining the nature of the transition metal and oxygen bond accompanied by three subsequent sections bridging the redox spectrum from pure anionic, mix of cationic and anionic and pure cationic.

Introduction

Lithium-ion batteries (LIBs) have been the centre of research attention for many years. Their application in portable electronics, electric vehicles, and drones among others have helped revolutionized humanity as a species.[1] As our desire for higher energy density energy storage devices have grown over the years, the need for higher performance battery have increased drastically. While there are many candidate technologies, such as Li-S,[2-4] Li-O_2,[5-8] Zn-air[9-11] and other multivalent battery systems,[12-15]etc., the field of LIBs holds much promise for further improvements in energy densities, while remaining in the realm of well-established LIB manufacturing infrastructure. Currently much effort is placed on moving towards low Co composition due to the high cost and geopolitical issues regarding Co supply. Li-rich cathode compositions of $Li_{1.2}Ni_{0.13}Mn_{0.54}Co_{0.13}O_2$ (low Co)[16,17] and even the Co-free cathodes[18,19] are quite attractive for the industry especially since they can theoretically offer higher energy density and lower cost. The mechanism from which the high energy density is achieved from lies in the reversible redox of the oxygen anions in addition to the metal cations.

Since the advent of Li-ion batteries, the transition metal oxides (TMOs) used as the active cathode material have been considered exclusively based on cation redox electrochemistry. That is the main redox centre in the TMO is the cation transition metal (TM). Only a few years ago have the phenomenon of anion redox electrochemistry been established and accepted to be occurring in TMOs for LIBs where the 2p-band of the oxygen overlaps with the d-band of the metal.[20] From modern spectroscopic characterization techniques, anionic-redox occurs due to the degree of which the O is bonded with the TM or the subsequent existent of O non-bonding-like orbitals in the TMO. When this occurs, these particular TMOs cathode material have comparatively higher capacity for Li-ion storage and consequently higher expected energy densities. However, the stability of the TMOs begin to quickly deteriorate with cycling due to structural collapse and the eventual release of gaseous oxygen.[20] It became clear that anion redox will most likely in the near future, be difficult to control. Accordingly, recent work have placed a larger emphasis on what is known as Li-excess cation-disordered rock salt[21] (or colloquially: DRX[22,23]) materials which are also expected to offer a large increase in energy density along with a higher electrochemical stability among the anion redox materials.

In less than a decade, research have progressed quickly into this field, establishing mechanism and knowledge frameworks[24 25]from which new materials can be based upon. While there has been a few reviews that have discussed the mechanism of anionic redox (AR) and the various materials,[24-27] recent major advances in the field (in the past year) have significantly transformed our understanding very quickly. Accordingly, it is timely to review this field in details for both comprehensiveness and correctness for the readers. Moreover, this field of science have offered an opportunity to merge parts of the various battery fields into a unified spectrum that have not been established by others. In this review we will bridge the discussion between pure cationic

[a.] *Chemical Sciences and Engineering Division, Argonne National Laboratory, 9700 Cass Ave, Lemont, IL 60439, USA.*
[b.] *Department of Chemical Engineering, Waterloo Institute of Nanotechnology, University of Waterloo, 200 University Ave West, Waterloo, ON N2L 3G1, Canada*
[c.] *School of Materials Science and Engineering,Tianjin University. 92 Weijin Road, Nankai District, Tianjin, China, 300072.*
[d.] *Department of Material Science and Engineering, Stanford University, Stanford, CA 94305, USA*
[e.] *Institute for Research and Medical Consultations (IRMC), Imam Abdulrahman Bin Faisal University (IAU), Dammam, 34212 Saudi Arabia*
* Footnotes relating to the title and/or authors should appear here.
Electronic Supplementary Information (ESI) available: [details of any supplementary information available should be included here]. See DOI: 10.1039/x0xx00000x

redox (CR), cationic and anionic mixed redox (CAR)[28] and pure AR[8,29] to establish a clear spectrum for these technologies. First, a discussion on the evidence and underlying reasons responsible for cationic and anionic redox will be presented. To follow will be section on CR, CAR and AR with discussion on some of the most relevant materials and designs.

Fundamentals of Anion Redox

Experimental Evidence for Anionic Redox Contribution in Li-ion Batteries

CAR and AR with discussion on some of the most relevant materials and designs. Anionic redox was originally an explanation for the extra capacity obtained from the delithiation a TMO. Studies regarding the change in the TM's valence established early on it was impossible that the TM was the only redox centre at certain voltages.[30] The term anionic redox refers to the actual existence electrochemically active electrons of the O atoms in the TMO lattice, from which the extra reversible capacity for Li insertion stems. Therefore, the existence of anionic redox must be accompanied by a change in the valence of the O atoms in the TMO. Although evolution measured by differential electrochemical mass spectroscopy (DEMS) likely represents the most clear proof for oxygen oxidation ($2O^{2-} \rightarrow O_{2(g)} + 4e^-$), it cannot be applied towards analysing reversible AR as there should be not O_2 evolution (which will inevitably occur in any TMO at an anodic enough potential).[28] Accordingly, most of the evidence for the anionic redox revolves around observing the change in the O valence when Li-ion capacity is extracted/inserted into the TMO. Early X-ray diffraction work by Tarascon *et al* have identified a peculiar reduction in the O-O spacing from the delithiation of $LiNi_{1-x}Co_xO_2$ (x=0, 0.3 and 1).[31] Further evidence from the Li_2IrO_3 system was found by a transmission electron microscopy study where structural changes in the delithiated material implied peroxide formation.[32] It was rationalized that similar to other chalcogenide-based intercalation hosts,[33,34] O underwent redox along with the TM that is, CAR. This was also backed by even earlier theoretical studies by Cedar where he proposed that the O redox is the dominating redox centres and not TM in some TMOs.[35]

Among the published work, perhaps the most convincing spectroscopic evidence for CAR stems from electron paramagnetic resonance (EPR), X-ray absorption spectroscopy (XAS) and resonant inelastic scattering (RIXS). As any O oxidation will likely create radicals from the oxidation of O^{2-}, EPR is an ideal technique for identifying such chemical species. Specifically, EPR was applied for the delithiation of $Li_2Ru_{0.5}Sn_{0.5}O_3$. At high charging voltages (4.6 V) as shown in **Figure 1a**, the EPR signal detected at a temperature of 4 K largely resembled that of calcium CaO_2, suggesting the oxidation of the lattice oxygen atoms from -2 to -1.[36] The use of soft XAS detected dramatic changes in the O K-edge over delithiation of the $LiCoO_2$. This is in contrast with the minor changes in the Co L-edge. From a fully lithiated system (spectrum denoted by x = 0.00) to a partially delithiated (x = 0.15-0.75), more distinct features began to develop around the O K pre-edge (~528 eV, shown in **Figure 1b**).[37] The A_1 peak related to the hybridization of the Co 3d and the O 2p orbital, decreased in intensity over the delithiation cycle, indicating a decrease in the Co-O bond covalency.[38,39] The authors reasoned that the appearance of other neighbouring peaks (A_2 and A_3) indicated the re-hybridization of the Co-O bonds due to the change in charge from delithiation. Other works[40] have generally stated that the A_{1-3} features are the hybridization features of the $Co^{3+/4+}$ with O-2p. Additionally, a slight shoulder peak appeared at a higher absorption energy level than A_1, which the authors attributed to the oxidation of O with delithiation. However, this attribution is in the end rather arbitrary and should be interpreted with caution. Taken together, these observations can only clearly say that the Co-O bonding environment has changed as a result of delithiation. However, a change in the O bonding environment does not necessary indicate AR and could simply mean the O is compensating for the change in oxidation state of its bonded TM. For example, it has been shown that a similar change in the pre-edge features have been identified in TMOs (olivines[41] and spinels[42]) that do not have AR. The pre-edge feature lies right in the energy regime that has been related to merely TM's contribution to hybridization. [43] Although the XAS results summarized here is not definitive in proving both CAR are present, it was encouraging and promoted future work for corroboration.

Perhaps a more appropriate technique is RIXS. RIXS can probes the energy profile of the emission spectrum of the TMO over a range of excitation energy.[44-46] This effectively expands the emission information in a XAS from 2D (count versus excitation energy) to 3D (count versus excitation energy and emission energy) that is, each point on the XAS absorption spectrum is expanded into its corresponding full energy-resolved emission spectrum, (analogous to the relationship between fluorescence emission and resonant Raman excitations).[27] Although the previous description is somewhat simplified and the corresponding data interpretation is in fact more complicated in nature, the benefit of expanding the spectroscopic data by this dimension lies in the ability of RIXS to clarify the pre-edge features and detect distinct fingerprint-like signatures that only appear in AR. As shown in **Figure 1c** with both CAR, a clear spike in intensity (indicated by a white arrow at an excitation energy of ~530.8 eV and an emission energy of ~523.75 eV for this study) is found at 4.8 V in the $Li_{1.2}Ni_{0.2}Mn_{0.6}O_2$ material, which disappears when discharged. Similar phenomenon was also found for recent work in Na-ion batteries with anionic redox.[46] This is in stark contrast with **Figure 1d** for $Li_{1.2}Ni_{0.2}Ru_{0.6}O_2$ (only CR is expected) where no spike in intensity is found.[45] If only XAS was performed, this extra peak at a different emission energy would be integrated along with the two adjacent peaks at an emission energy of ~525 eV, forming a convoluted signal. Importantly, this RIXS signature was also present in independently captured RIXS maps of Li_2O_2.[47] In the same work, the authors mapped both Li_2O and Li_2CO_3 as comparison, suggesting that the unique signatures of Li_2O_2 and the O in AR-active TMOs are related to the partial filling of the oxidized O 2p bands. It is important to point out that similar RIXS features (around an excitation and emission energy of ~530.8 and 523.5 eV respectively) was also found for molecular oxygen.[48] This is indicates that there is still much left to be understood in the use of RIXS to prove AR. Specifically, RIXS should still be interpreted with caution, while a deeper understanding in to the RIXS phenomenon and the impact of the TM on the O RIXS signatures should be pursued by the research community.

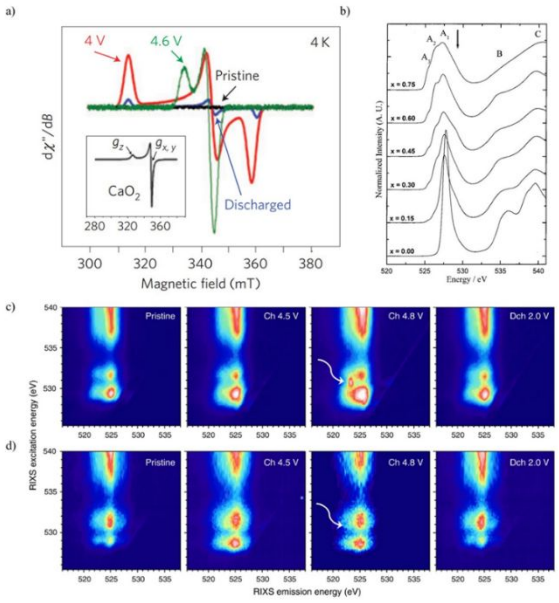

Figure 1: a) Electron paramagnetic resonance spectroscopy (EPR) of $Li_2Ru_{0.5}Sn_{0.5}O_3$. Reproduced with permission.[36] Copyright Springer Nature 2013 b) Change in the O K-edge measured by soft X-ray absorption spectroscopy (XAS) at various degrees of delithiation of $Li_{1-x}CoO_2$ in which case x is the degree of delithiation. Reproduced with permission.[37] Copyright The American Chemical Society 2002. O K-edge resonant inelastic X-ray scattering (RIXS) excitation energy (eV) vs emission energy (eV) contours plots as a function of voltage for c) $Li_{1.2}Ni_{0.2}Mn_{0.6}O_2$ (anionic redox) and d) $Li_{1.2}Ni_{0.2}Ru_{0.6}O_2$ (no anionic redox). Reproduced with permission under the Creative Common License Deed.[45]

Overall, the evidence for anionic redox has been mainly obtained by a combination of X-ray diffraction (XRD),[31] X-ray photoelectron spectroscopy (XPS),[36,49] XAS,[37,45,50,51]RIXS,[27,45] EPR[29,36] and differential electrochemical mass spectroscopy (DEMS).[29,36,45,50,52] Briefly, XPS, RIXS and XAS can provide information pertaining to the valence of the O in the TMO where RIXS mapping can offer energy-resolution for the excited energy states. EPR serves as mean to detect the created peroxide radicals. The eventual evolution of lattice O in the form of O_2 is then detected by DEMS. Taken together, these characterization techniques have convincingly indicated that CAR is occurring in some TMOs and have built the foundation upon which new CAR materials will be validated and identified. The following sections will discuss about how these techniques have been used to formulate the mechanism of CAR.

Mechanism of Anionic redox

Over the research history of this anionic redox, there has been many different theories on what exactly renders specific TMOs CAR active and reversible. While they are all describing the same phenomenon, some of them differ significantly from one another. In this section we will discuss these mechanisms and descriptors for reversible CAR in Li-rich layered material and disordered rock salt materials while noting their relevance in the current CAR literature. Early theory for the extra capacity present at higher charging voltage included theories such as the over metal oxidation up to Mn^{5+},[53] or the extraction of the Li_2O units from the Li_2MnO_3, activating additional capacity.[54] The majority of these alternative theories have been listed and summarized by Tarascon *et al*.[24] However, it is important to point out the difference between AR from over-delithiation of common systems such as LCO. O_2 evolution is a result of the oxidation of O anions and is not reversible in nature in a LIB configuration. Accordingly, this type of electrochemistry is not useful for a battery and is not considered AR. The type of O electrochemistry that is considered AR entails relatively reversible O redox with specific mechanisms.

Firstly, from XAS studies, many researchers have thought that the CAR is related to static O^{2-}/O^- redox couple.[55,56] Perhaps the main school of thought for AR generally stems from the existence of O 2p lone pairs in the TMO. When O is bonded to TM and Li, there will be the formation of TM-O bonds that may or may not form lone pairs depending on the valence of the TM and the ratio the elements. Furthermore, the AR is likely not a perfect O^{2-}/O^- redox couple as in the case of Li_2O_2 formed in lithium-O_2 batteries,[57] but instead forms oxidized O in the form of peroxo-like O_2^{n-} dimer species[32,36] or isolated O^- anions.[19,55,58] These two possible scenarios are also often coupled with change in the crystal structure of the TMO. It is important to show that the physical location of AR redox sites and the corresponding change in the TMO crystal structure occurred throughout the bulk of the TMO particle. While this might appear to be a rather trivial matter, its confirmation was not particularly simple without certain characterization techniques. Typical XAS measurement obtains a bulk average of the sample. Therefore, only by a specialized spatially resolved analysis techniques can the bulk redox of O be analysed.

Much of the spectroscopic studies regarding AR did not take into account the concurrent changes in the structure of the material as proven via transmission electron microscopy[59,60] and, neutron[61] and X-ray[59,62,63] scattering/diffraction experiments. By using a transmission X-ray microscopy with nanoscale X-ray absorption, the delithiation of $Li_{1.17-x}Ni_{0.21}Co_{0.08}Mn_{0.54}O_2$, or specifically the mechanism of CAR of this material was found to be related to the removal of electrons from the TM 3d-O 2p hybridized orbitals at voltages below 4.5 V followed by the oxidation of just O 2p above 4.5 V.[64] As this technique is spatially resolved, oxidation above 4.5 V was readily concluded to be related to the migration of the TM throughout the entirety of the TMO particle and not just the surface. This offers a correlated structural and spectroscopic explanation of CAR, indicating that when the O redox is active (>4.5 V), there must be a corresponding reaction that likely simultaneously occurs causing TM migration. This is also complemented by XPS performed with hard X-rays where higher penetration is achievable.[49] By increasing the energy of the X-ray, the penetration depth the XPS increase from 6.3 nm at 1.487 keV to 13 nm at 3.0 keV and 29 nm at 6.9 keV. To ensure 29 nm was deep enough to be considered bulk, the author utilized Li-rich NMC with a particle size of ~100 nm. The authors found that the percentage of O^{n-} present over the total amount of $O^{n-} + O_2$ did not change when moving deeper into the sample, indicating the AR is a bulk process. In fact the signals from the sample at a higher depth were less convoluted due to the lack of electrolyte decomposition product. Additionally, 3D electron tomography reconstruction also revealed an increase in pore volume inside the $Li_{1.2}Ni_{0.15}Co_{0.1}Mn_{0.55}O_2$ particle over cycling as shown in **Figure 2a** (pristine) and **Figure 2b** (after 15 cycles).[28] These pores are believed to stem from the nucleation and accumulation of O vacancies from O_2 evolution. The pore fraction varied from 1.5 to 5.2% (relative to entire particle volume). When taken together, these experimental results provide the most concrete evidence that AR is not just a surface phenomenon but occurs throughout the bulk of the TMO

particle.

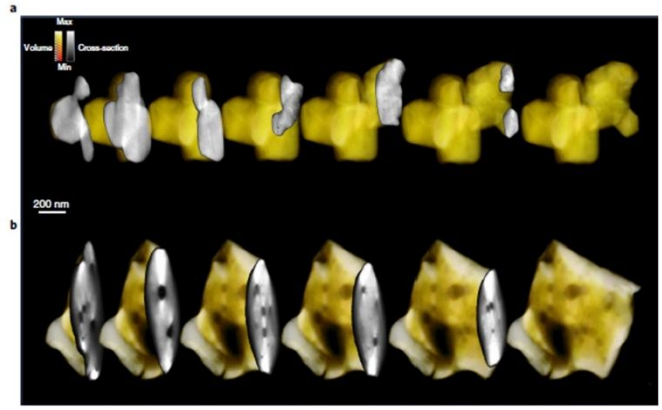

Figure 2: 3D electron tomography reconstruction of $Li_{1.2}Ni_{0.15}Co_{0.1}Mn_{0.55}O_2$ with cross section in black/white and volume in green during a) pristine state and b) after 15 cycles. Reproduced with permission.[28] Copyright Springer Nature 2018.

The most widely accepted reason for the extra-capacity has been established to be from the O atoms acting as redox centres. For Li-rich layered materials, the mechanism of anionic redox have been described by many groups to be based on the degree in the covalency of the TM-O bond. Due to this covalency, the Fermi level state degeneracy is split into the similar energy level of O 2p and TM d-band.[20] When Li-ions are removed, both O and TM can act as oxidation sites for providing the electron to the external circuit. However, because O is so electronegative, compounds consisting of TM and O usually results in clear separation between the O 2p-band and the d-band of the TM (typically the redox active centre for pure CR materials). Generally, relatively reversible CAR can be achieved by using less electronegative anions or using TM such as Ru and Nb among other TM that possess a 4d band.[65] The 4d or higher bands allow for more covalent bonding due to their larger orbital sizes. If ones looks towards the other chalcogenides, the nature of the bond are also correspondingly more covalent with more overlap between the O 2p and TM d band.[34] Specifically, if O was to be replaced with S, the higher polarizability and overall lower iconicity of S would also allow for anion redox as exemplified by the Li-ion de-intercalation from Li_2FeS_2.[66]

Research groups have developed CAR reversibility and capacity descriptors based on covalency-based parameters of the material. The ratio between the Coulomb interaction term U and the charge transfer term Δ_{CT} has been proposed by Doublet *et al* as rough descriptor without true exact values.[67,68] U is a value used to describe the Coulombic repulsion between two atoms (charged entities) depending on its electron density and the radius of the atoms. Generally, the greater the U, the smaller the size of the atoms. Δ_{CT} is the charge transfer between the two atoms in the compounds. The greater the charge transfer, the greater the ionic characteristic of the bond. If $U << \Delta_{CT}$ (known as a material in the Mott-Hubbard regime), the TMO of interest will undergo mostly a CR and the system is very ionic. If $U >> \Delta_{CT}$ (known as a material in the Charge Transfer regime), the system will undergo mostly an irreversible AR.[69] The intermediate regime where $U/\Delta_{CT} \sim 2$, the system will have both the MO^* d-band and the O 2p lie in the Fermi level and the system will undergo both CAR. When this occurs, the O 2p-bands becomes electrochemically active and will undergo redox at higher voltages. The degree of covalency of the M-O bond will dictate the energy level of the non-bonding O 2p lone pair and correspondingly, the electrochemical activity and reversibility of this non-bonding O 2p. For example, if the formed $(O_2)^{n-}$ peroxo-species cannot be bonded to or stabilized by the TM, there will be irreversible O_2 gas evolution.[20] The stabilization of the peroxo-species occurs through what is known as a reductive coupling mechanism that is,[69,70] the TM is reduced while the O is oxidized.

When AR occurs, the electrons removed from the TMO stems from the O (i.e. AR). After $2O^{2-}$ are oxidized by the removal of 2 Li-ion and 2 electrons, a single $(O_2)^{2-}$ peroxide species would form. This is coupled with the splitting of the O 2p into σ, σ^*, π and π^* with their energy change denoted as $\Delta^{\sigma}_{O\text{-}O}$ and $\Delta^{\pi}_{O\text{-}O}$ for the sigma- and pi-bond states respectively (as shown in **Figure 3**).[71] The $(O_2)^{2-}$ peroxide species must now be charged balanced with the TM *via* the reduction of the TM (i.e. reductive coupling mechanism). If the TM cannot appropriately undergo the reduction process, the system will destabilize, leading to O_2 gas evolution.[20] How well the TM can undergo the reduction can be viewed by the Δ_{CT} energy (difference in energy between the lowest TM d band and the O 2p). When Δ_{CT} remains greater than $\Delta^{\sigma}_{O\text{-}O}$ (left of numbered 1 blue circle in Figure 2), the system will generally undergo stable anionic redox. If the anionic capacity is increased towards right of the number 2 blue circle ($\Delta_{CT} < \Delta^{\pi}_{O\text{-}O}$), the system will evolve O_2 irreversibly. In between the number 1 and 2 blue circle, the system will still produce voltage hysteresis, but in this region the TM are expected to stabilize the peroxo-species. Overall, as more and more Li-ions are stripped from the system, the O 2p becomes more and more distinct from the TM's d-band with the eventual release of O_2. Interestingly, if the mechanism described for AR and CR is only related to the covalency of the TM-O bond or their hybridization, the total capacity of the system should still not exceed that of the theoretical limits predicted from the TM.

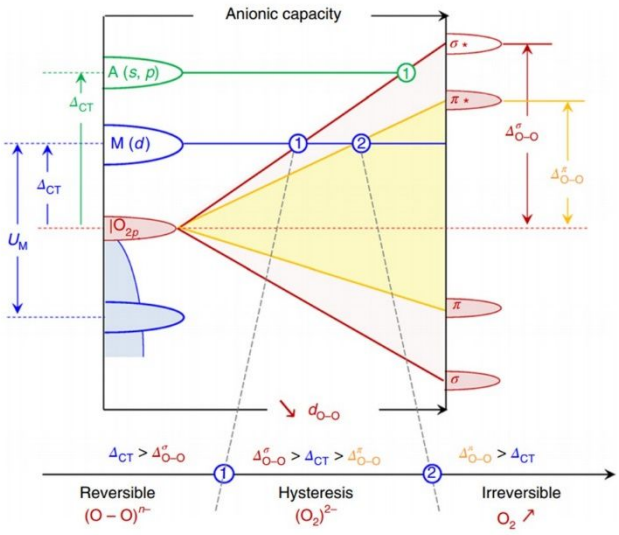

Figure 3: Qualitative electronic structure of TMO with reversible, hysteresis and irreversible anionic redox. Vertical axis denotes the relative energy levels and horizontal axis denotes the decrease in bond distance between O-O or increasing anionic capacity from left to right. Reproduced with permission.[71] Copyright 2019. Springer Nature.

Another method for gauging the degree of reversible and extent of CAR is the ratio of Li and TM and the existence of a particular linear Li-O-Li bond. This method is distinct from just the TM-O covalency and allows for additional capacity from the O that is not intrinsically coupled with the TM. Cedar *et al* demonstrated that when one replaces the Ni in $LiNiO_2$ with Li, the projected density of states (pDOS) for the O 2p changes drastically when Li is added (**Figure 4a-c**).[55] Specifically, the change from 3 Li with 3 Ni (Figure 4b) to 4 Li to 2 Ni (Figure 4c), the O 2p pDOS exhibited an increase between 0 to -2.5 eV from the Fermi level. They reasoned that this increase in DOS stems from the formation of a Li-O-Li linear bond as shown in **Figure 4d**. Of the two O 2p orbitals, the one along the Li-O-Li and not the Li-O-TM is key to the AR capability of the TMO. O 2p orbitals in the along the Li-O-TM bond are hybridized with the TM which produces the same states as the stoichiometric layered oxides. For the Li-O-Li bond, the O 2p will not hybridized with the Li due to too great of an energy difference which forms orphaned O 2p states. These orphaned O 2p states are then positioned in the TM-dominated complex of e_g and t_{2g} states of the TM. When this occurs, the O 2p in this configuration are particularly labile and redox active, even making AR and CR compete with each other. Similarly, the authors theorized that since many of the CAR TMOs are achieved by increasing the Li to Ni ratio in the sample that is, Li-rich/Li-excess TMOs, the same rationale was used to explain the CAR phenomenon between other Li-rich TMOs. For example, in Li_2MnO_3 (**Figure 4e**), the same linear Li-O-Li bonds are produced increasing the O 2p DOS (**Figure 4f**). Furthermore, the Li atoms participating in the linear bonding with O are the ones that are active when AR occurs. This method can be used to explain the CAR properties of both Li-rich layered TMOs and disordered TMOs. This explanation is different from the previously described dependence of the nature of the CAR on the covalency of the TM-O bond. In contrast, it was explained that the unhybridized O 2p are the key electrons useful for AR. From this viewpoint, the amount of oxygen redox does not change the available TM redox in terms of capacity (but still in terms of delithiation potential due to hybridization[72]). In fact, from this perspective, the AR redox are somewhat decoupled from CR. The ordering of AR or CR or simultaneous CAR will proceed based on the d states of the TM species. This is reflected in the O redox difference between $Li_{2-x}IrO_3$ (multivalent Ir redox compensated by O redox) and $Li_{2-x}Ir_{1-y}Sn_yO_3$ (additional capacity from O redox).[44] Furthermore, by changing the TM species, the system's redox active d-band of the TMO can be changed to either ensure that AR also occurs at a similar voltage or only after CR. Furthermore, if the energy levels of the TM were to be raised higher than that is preventing TM and O orbital overlap, the amount of TM can be maximized in Li-rich TMOs.

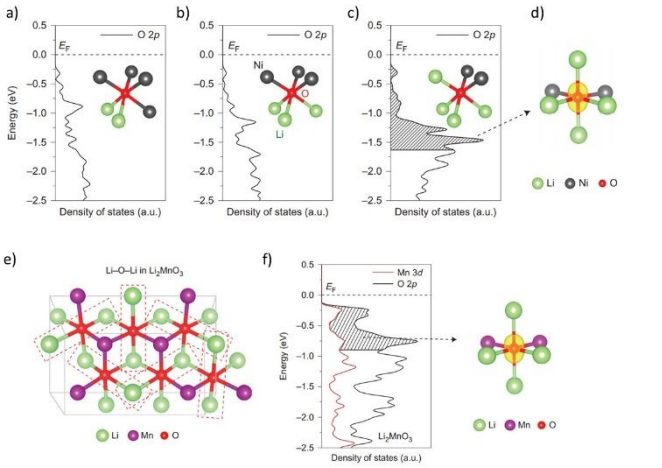

Figure 4: Projected density of states of a O coordinating environment of a) 2 Li/4 Ni, b) 3 Li/3Ni and c) 4 Li/2 Ni. d) Rotated view of the 4 Li/2 Ni configuration illustrating the characteristic linear Li-O-Li bond (highlighted). e) Structure of Li_2MnO_3 with the Li-O-Li indicated with boxed dotted lines. f) Projected density of states of Li_2MnO_3 for Mn 3d and O 2p. Reproduced with permission. [55]Copyright Springer Nature 2016.

Beyond just Li-rich systems and the regime of which the TMO falls upon (Mott-Hubbard or Charge Transfer) or degree of covalency, Doublet *et al* very recently suggested that the holes per oxygen was a more universal and accurate indicator of reversible CAR.[71] This method moves beyond the crystal and electronic structure of the material and becomes more generic or intrinsic to the underlying phenomenon. Whether the system is disordered or substituted, the underlying effect on the AR is the resulting distribution of the non-bonding O 2p. The unhybridized O 2p will be entirely dependent on the electrostatic environment generated from the adjacent atoms to O as it is not bonded. Generally, a hole on the O sublattice (h^o) numbered <x is required to maintain reversible AR. In this case, x denotes the excess Li present in the TMO with the generic formula $Li[Li_xM_{1-x}]O_2$. The value of h^o depends on how homogenous the O network is and the amount of theoretical anionic capacity available. The maximum number of electrons to be removed with Li-ions will then be 1+x. While the Δ_{CT} can be used to estimate how much extra capacity will stem from AR, h^o requires both the Δ_{CT} and x, which can be used to quickly estimate whether the candidate TMO will have reversible AR. If h^o remains below x, the majority of the capacity will stem from cationic redox in a reversible fashion. Changing h^o can be achieved by changing the amount of electrochemically inactive TM into the TMO. For example, β-Li_2IrO_3[73] and Li_2RuO_3[74] has no electrochemically inactive TM elements. For these TMOs (h^o <x), the CAR has been shown to be quite reversible and usually exhibits distinct plateaus for CR and AR as schematically shown in **Figure 5a** with relatively negligible hysteresis. If a non-electrochemically active TM is substituted into the TMO, the h^o will shifts towards a higher number (as shown in **Figure 5b**). This is the most common situation among researched materials[32,36,60,75] where irreversible capacity is observed along with higher voltage hysteresis and cycling occurring with an S-shaped curve. In some situations, the AR process would activate some CR that was not previously available which would compensate for the loss in AR (**Figure 5c**). When all of the electrochemical active TM are substituted for inactive TMs and h^o= (1+x)/2, the Li-rich TMO will experience O_2 evolution with voltage fade on each cycle as shown in

Figure 5d. The critical number of holes per oxygen appears to be 1/3. At this level, no O_2 release will occur.

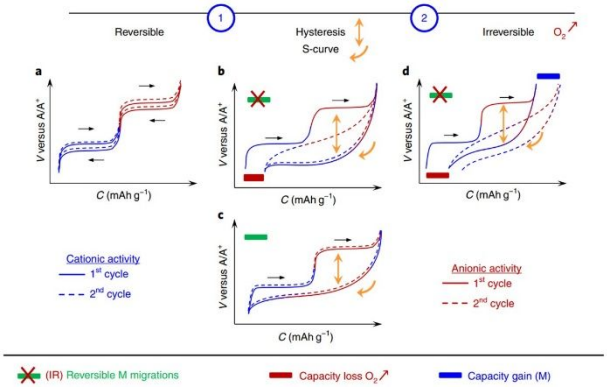

Figure 5: The four generic types of CAR. a) Homogenous system with $h^o<x$ where the system is highly reversible with no capacity loss from O_2 evolution. b) $h^o=x$, with oxygen release leading to irreversible capacity loss on discharge. This is the most common Li-rich TMO reported in literature. c) $h^o=x$, but with the development of new TM redox pairs that can compensate for the capacity loss from O_2 evolution. d) $h^o>x$ results in irreversible capacity loss from O_2 evolution and persistent voltage fade. Note the blue and red portion of the voltage profiles represent the cationic and anionic contribution respectively. Reproduced with permission.[71] Copyright Springer Nature 2019.

The Spectrum of Cationic and Anionic Redox

As described in the previous section, the process of CR and AR are both fundamentally linked to the nature of the h^o. This is a generic statement that is meant to offer the research community a means to predict and gauge the CAR in a given compound. Now we will discuss specific material and battery technologies that have mostly AR, a blend of CAR and mostly CR. As the most basic and pure for anion redox, Li-S and Li-O_2 will be discussed in terms of leveraging the possibility of state-of-charge control of pure anion redox. This is in contrast to their full conversion reaction, which are practically very difficult to achieve reversibly. Cationic and anionic combined redox will be discussed with regard to some of the early materials and current state-of-the-art materials. Cationic redox will discuss Li- and Mn-rich layered materials, disordered rock-salts and their variations TMOs.

Anionic redox

Over the develop timeline of the anionic redox field, its definition have evolved significantly. Currently, what is considered AR is the reversible depopulation of the non-bonding O 2p states where the create electron holes in the O 2p remains in orbitals that possess O characteristics even after the structural and electronic restructuring throughout delithiation. However, it is likely this definition will continue to evolve as research progresses. Whether or not something should be classified as AR will remain open to discussion among the research community. However, some of the recent work in the field of Li-O_2 remains to be undeniably some extreme form of AR where there is a full substitution of redox active TM for Li. While Li-O_2 typically do not have TMs to enabled the same kind of AR,[5] this section will discuss some of the more unique form of Li-O_2 battery recently demonstrated with future implications in Li-S and potential of this class of battery proposed.

Li-O_2 and Li-S batteries

Li-S and Li-O_2 batteries are 100% AR and have significantly different characteristics than CAR and CR. Fundamentally, the lithiation of S_8 or O_2 are known as conversion reactions. There are no intercalation of Li-ions into the crystal of either of these chalcogenides as there are in the case of the conversion reaction based TMO anodes. While the conversion reaction mechanism of TMO of pure chalcogenides leads to significant problems in terms of cycle stability and Coulombic efficiency, they typically possess immense potential in both specific and volumetric energy density. Overall, both of these systems have mostly been considered for their full redox reaction from an oxidation state of 0 to -2 or -1 (in the case of Li_2O_2). As both Li_2O and Li_2S are ionic compounds, the bond between the Li-O/Li-S is very strong. This could be seen as an extreme case of no TM substitution compared to the CAR and CR materials. Because of this strong bond and the corresponding poor ionic and electronic conductivity, it is very difficult to strip the Li-ions from Li_2S/Li_2O particles. In the case of Li_2S, it has even been accepted that the outer shell of the Li_2S particle will be stripped of Li-ions forming high oxidation compound that is, the Li_2S particles does not charge in a sequential manner (in terms of oxidation state) like the common TMO.[76] If the anion redox of these compounds were to be consider in the same sense as the CAR and CR compounds, there should be some ability of the system to achieve partial conversion, that is avoiding the full oxidation of S/O from a state of -2 to 0.

The benefit of a partial conversion reaction for S and O based systems i.e. controlling the state of charge (SOC) of the system, is the enhanced cycle stability of the cell. However, work on limiting their redox to prevent full conversion remains to be rare and could be one of the key direction in the future.[77]For example, early work showed that pure solid LiO_2 can be relatively stable, which could then be used independently in a Li-ion battery based set up.[8] More explicitly, work on a pure anion redox nanolithia was recently shown to be quite stable as a partial Li-O_2 battery even in carbonate-based electrolyte.[29] This work demonstrated that when Li_2O is small enough and there is a catalyst (through some unclear mechanism) as schematically shown in **Figure 6a**, it is possible to achieve partial oxidation from O^{2-} to O^x where x ~-0.5. Shown in EPR (**Figure 6b**) and Raman (**Figure 6c**), there are convincing evidence that LiO_2 species are present in the sample after charging to 600 mAh g^{-1}. A voltage plateau was found at around ~2.5 V, which is exactly the cell voltage of a low overpotential Li-O_2 as shown in **Figure 6d**.[78] Similar results were found for Co-doped Li_2O[79] and nanolithia embedded into an Ir-graphene catalyst host.[80] Because the SOC was controlled to not allow for O_2 release, the Li-O_2 discussed here is much more stable (up to 200 cycles). Whether it is a simple particle size dependent phenomenon or there is some nonbonding O 2p from bonding with the Co_3O_4 skeleton or a combination of both remains to be answered. However, it was theorized that Ir-graphene based nanolithia redox was achieved because the unstable delithiated Li_2O's outer shell can be stabilized by the oxidization of Ir, forming a $Li_{2-x}O_2$-Ir compound.[80] Validation of this theory will require further extensive studies.

Pure Li_2O can be viewed as the completely substituted form of Li TMOs (Li substituted TM) where there also exist linear Li-O-Li. The key difference could lie in the lack of electron and ionic conductivity throughout a bulk Li_2O, which might limit its electrochemistry to surface reactions. As nanonization of Li_2O will likely have tap density problems later on in the prototype stages, future probing into whether or not there

exist any bonding between the Co_3O_4/Ir-graphene framework and the Li_2O to enhance the electrochemistry of the system is key to any future commercial breakthrough.

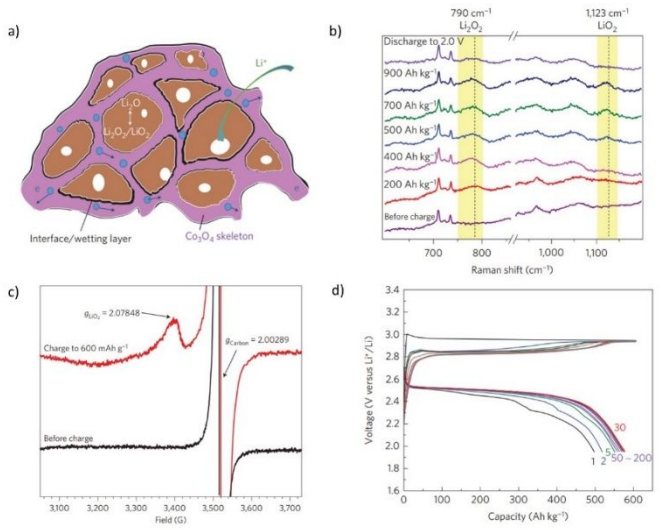

Figure 6: a) Schematic illustrating the distribution of Li_2O among the Co_3O_4 skeleton/framework. b) Raman and c) electron paramagnetic resonance spectroscopy of the cathode at different state of charge. d) Voltage profile of the nanolithia composite at various cycles. Reproduced with permission [29]Copyright Springer Nature 2016.

Interestingly, in terms of Li-S batteries, there has not been any reported work that was able to limit the direct oxidation of Li_2S to Li_2S_8/S_8. It has been well-established that the charging mechanism of Li_2S entails the initial delithiation of the surface of the Li_2S particles forming high order Li_2S_8/elemental S_8.[76] The highly soluble Li_2S_8 then reacts chemically with the remaining Li_2S through comproportionation reactions, forming lower order polysulfide species. As these polysulfide species are highly soluble in the electrolyte, they can be easily oxidized to Li_2S_8 or even to S_8. These electrochemically formed high order polysulfide species will then once again comproportionate with the remaining Li_2S.[81-83] In contrast to the oxidation of nanosized Li_2O,[29] the use of nanosized Li_2S did not offer a different charging mechanism (albeit without a metal or metal oxide catalyst to stabilized any delithiated species).[84] A characteristic of a polysulfide formation when charging Li_2S is the initial activation peak. In the case of a nanosized graphene-encapsulated Li_2S (as shown in the transmission electron micrograph in **Figure 7a**), there still exist a sharp increase in initial overpotential up to ~3.25 V (**Figure 7b**), indicating the direct formation of high order polysulfides from Li_2S.[83] This suggests that the same SOC control for Li_2S cannot be achieved by simple nanonization down to ~50 nm particles. However, further decreasing the particle size down to $Li_{20}S_{10}$ was theoretically predicted to possess extremely low overpotentials.[85] Interestingly, amorphous Li_2S film synthesized from a vapour-phase atomic layer deposition method was shown to produce a 1st charge voltage profile that still exhibited a slight overpotential resulting in a cell voltage of ~2.4 V vs Li/Li^+.[86] By enabling an oxidatively sequential charging mechanism in Li_2S, the formation of polysulfides could be avoided based on a SOC control (analogous to common TMO for LIBs) and thus likely produce a more stable Li-S battery. A similar aforementioned Co_3O_4 catalyst framework [29] could also benefit the controlled sequential charge of Li_2S. However, this type of AR (if it can be allowed to be considered as such) still requires much additional work and understanding.

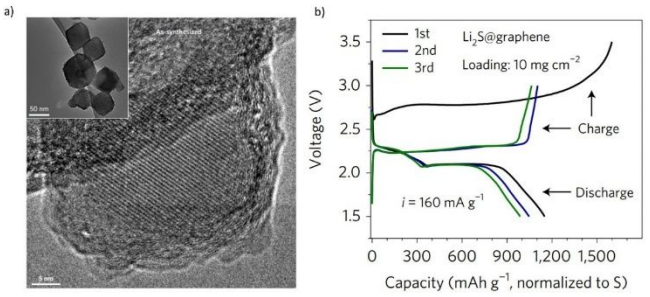

Figure 7: a) Transmission electron micrograph of the nanosized graphene wrapped Li_2S with low magnification image shown in inset and b) the corresponding 1st, 2nd and 3rd cycle charge/discharge voltage profile. Reproduced with permission. [84] Copyright Springer Nature 2017.

Reversible cationic and anionic redox:

A material with a mixed reversible CAR can occur in different situation. Although the overarching mechanism is more or less the same that is, the existence of non-bonding O 2p orbitals, the specifics of the cycling varies. In this section, we will discuss the details of some of the leading CAR TMOs under the two major classes of materials: Li-rich layered cathodes and Li-excess disordered rock salts. Under these sub-headings, specific major technologies and research fields will be discussed in detail.

LI-RICH LAYERED CATHODE MATERIALS:

$LiNi_{1/3}Mn_{1/3}Co_{1/3}O_2$ (NMC111), a non-Li-rich material have played a key role in the electric vehicle market. However, prior to its discovery, Li-rich material have already been explored by Dahn *et al* in the form of $Li[Ni_xLi_{(1/3-2x/3)}Mn_{(2/3-x/3)}]O_2$ where x=1/3,5/12 and 1/2.[87] When x=1/2 the system reduces down to a non-Li-rich material ($LiNi_{1/2}Mn_{1/2}O_2$). For the other values of "x", the system is Li-rich and demonstrated very high capacity (~260 mAh g^{-1} at first cycle and ~200 mAh g^{-1} at 55 cycles) when cycled from 2.0 to 4.6 V at x=1/3 ($Li[Ni_{1/3}Li_{1/9}Mn_{5/9}]O_2$). It was not well understood that reversible anion redox was responsible for the enhanced capacity, but that the extra capacity was from evolution of O_2.[88] Thackeray[54] also separately investigated NMC material with an excess amount of Li. Li-rich layered oxide, have been long understood to be a specific type of TMO that possessed particular high capacity and thought to be a class of material that consisted of $LiMO_2$ (where M=Mn, Ni, Co) and stabilized by Li_2MnO_3.[54,89] The main problems involved with Li-rich layered oxides were their low first cycle Coulombic efficiency, poor energy density stability and poor rate performance.[90] While the capacity retention was relatively good, the energy output decreased quickly over cycling due to a well-known voltage fade phenomenon. It was not well-understood that AR was the cause of its capacity increase and poor durability.[91] This type of anionic redox materials were in fact the first ever demonstration of reversible (to some degree) CAR.

$Li[Li_{0.2}Ni_{0.2}Mn_{0.6}]O_2$ were once again revisited but with a specific focus of taking advantage of the anionic redox of the material.[19] This type of material consisted of layered structure of Li_2MnO_3 and $LiNi_{0.5}Mn_{0.5}O_2$[92]

and were particularly attractive due to their lack of Co which has been a pressing concern in terms of cost and global supply chain.[93] Interestingly, the use of isotope labelling of the lattice O atoms was used to determine if these O atoms were stripped from the TMO and evolved as O_2 or CO_2.[19] $Li[Li_{0.2}Ni_{0.2}Mn_{0.6}]O_2$ labelled with $^{18}O_2$ was prepared by heating the atmosphere in an $^{18}O_2$ atmosphere with a final proportion of 15.4%. Like most TMO cathodes, no O_2 evolution was detected below 4.5 V. Above 4.5 V oxygen release was observed. The authors stated that the e_g states of the octahedral Ni^{2+} were first oxidized, bringing $Ni^{2+}(t_{2g}^6\ e_g^2)$ $\rightarrow Ni^{4+}(t_{2g}^6\ e_g^0)$. This dropped the energy level of e_g and raised the O 2p, allowing for its redox upon further delithiation of the TMO. The CAR mechanism and the subsequent implication on the cycling is perhaps more deeply studied in the common material of $Li_{1.2}Ni_{0.15}Co_{0.1}Mn_{0.55}O_2$ (LMR). LMR was thoroughly investigated with a suite of characterization techniques throughout the past few years. The redox couple of TM and O was observed experimentally to change in proportion between one another drastically over cycling. Specifically, the change in oxidation state was observed via XAS at the Mn, Co, Ni and O K-edge of electrode cycled to different cycle number (1st, 2nd, 25th 46th and 83rd) at both charged and discharged states. Over the course of cycling, the edge position of Mn, Co and Ni was used to correlate to their oxidation state.[58] As there was an excellent linear relationship between the oxidation state and the edge energy of Mn, Co and Ni. The TM's change in oxidation can be easily deduced. The total charge contribution of the TM's to the capacity is then subtracted from the total measured capacity, obtaining the semi-quantitative contribution of O redox. As shown in **Figure 8a**,[28] the total capacity changed slightly (degradation mostly occurs in the form of voltage) from 1st to 83rd cycle. However, the proportions of Mn and Co were found to increase over the course cycling whereas Ni and O decreased. The decrease in Ni redox can be readily explained by the formation of an electrochemically inactive rock-salt phase on the surface.[94] The voltage fade is due to the change in the density of state of the cathode caused by the TM migration within the cathode to empty Li sites[60,64] due to the O redox. With the instigation of the Co^{2+}/Co^{3+} and Mn^{3+}/Mn^{4+} redox pair (which compensated the capacity decrease of Ni and O), the Fermi level of the system is raised and as such, the observed voltage drops or fade(**Figure 8b**). This is the exact type of material that exhibits the charge/discharge voltage profile shown in Figure 5c. It was argued that the reduction of the transition metal led to the weakening of the covalency on the TM-O bond and ultimately the proportion of O redox. However, regardless of the perceived mechanism, it was well recognized that the stability of these Li-rich layered TMOs were practically useless due to the voltage fade phenomenon (as in the case of Li-rich NMC[91]).

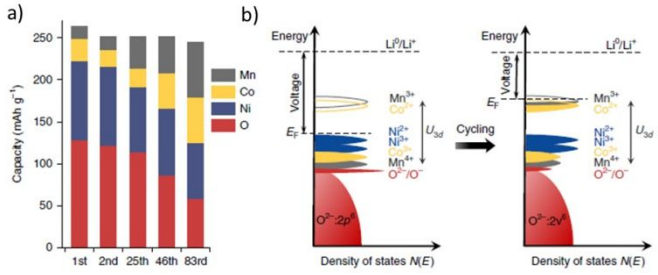

Figure 8: a) Evolution of capacity contribution of Mn, Co, Ni and O. b) Change in electronic structure of $Li_{1.2}Ni_{0.15}Co_{0.1}Mn_{0.55}O_2$ over cycling. Reproduced with permission.[28] Copyright Springer Nature 2018.

In most cases, and especially in early iterations of this class material, the stability of the AR was poor. O_2 release was very common at higher charging voltages, which directly correlated with poor cycle stability. Some work have focussed heavily on limiting the evolution of O_2 by surface coating the TMO with materials such as AlF_3,[95,96] MgO,[97] Al_2O_3,[98,99] $AlPO_4$,[100] and even polymers such as poly(3,4-ethylenedioxythiophene) polystyrene sulfonate (PEDOT:PSS).[101] This coating was found to limit electrolyte decomposition over the cathode (forming a cathode electrolyte interphase, CEI) and the surface phase transition from layered to spinel. In addition to coatings, suppression of O_2 evolution can be achieved more readily throughout the entirety of the LMR particles by doping with other metals.[90,102,103] These foreign elements have cumulative effect of enhancing the conductivity and overall stability of the TMOs. For example, Na-ions were shown to have a pinning or pillar effect where the added Na-ion can prevent the migration of TM ion into the Li-ion sites.[103-105]

To stabilize the O redox, it was found that substitution of the commonly used 3d TMs with 4d or even 5d TM have significant and desirable impact on the stability. The key difference between >4d over 3d electrons lies in their ability to make strong covalent bonds where the 4d electrons overlaps with that of the ligand nonbonding O 2p orbital. Initially, $Li_2Mn_{1-x}Ru_xO_3$ was synthesized to take advantage of the discovered higher capacity of the chemically leached Li_2MnO_3 by Thackeray.[106] Li_2IrO_3 was synthesized and found to have good electrochemical stability and capacity (~130 mAh g^{-1}) when cycled from 3.0 to 4.4 V vs Li metal.[107] Although enhancements in performances were obtained, the underlying reason is not well-known. Tarascon *et al* supported the sequential CAR theory via EPR and XPS analysis of $Li_2Mn_{1-x}Ru_xO_3$ with Mn substituted by Sn.[36] This was done to ensure that the extra capacity obtained by AR was not convoluted by the uncertainty of Mn redox. Sn was significantly more difficult to reduce to Sn^{2+}. The material was found to possess about 220 mAh g^{-1} in discharge specific capacity, significantly higher than most reported materials. Furthermore, it was quite stable up to 60 cycles with a specific capacity of ~200 mAh g^{-1}. By calculating the theoretical capacity of Ru^{4+}/Ru^{5+} redox, it was clear that O must be a significant redox center as well. Peroxo-like O species were found *via* XPS and EPR. The authors reasoned that the 4d orbital of Ru overlapped strongly with the 2p orbital of O. The delithiation process at 4.25 V and past it will therefore affect the O 2p levels, rendering them as redox centers. The detected peroxo-like O was reasoned to be formed from the generated O^- anions, which re-stabilized to O-O bonds. Furthermore, a later work also by Tarascon *et al*[73] revealed that the β-Li_2IrO_3 (5d TM) possessed exceptional cycle stability and specific capacity. β-Li_2IrO_3 consisted of a 3D long-range ordered framework of Ir-O bonds in a hyperhoneycomb structure. This structure possessed edge-sharing IrO_6 octahedra, which were able to accommodate the anionic distortion during AR. Experimentally, the structure was shown to remain stable up to a Li extraction/insertion process of 2.5 Li per TM with nearly no hysteresis.

Although the mechanism is open to debate, it was clear that 4d and 5d TMs were ideal for achieving enhanced performance with CAR. It is however unfortunately that these TMs were typically very expensive

and rather rare in the Earth's crust, rendering them impractical for commercialization. Alternative methods include substitution of Co with Fe in Li-rich NMC have shown to be beneficial towards suppressing oxygen release while increasing the stability of the redoxing O in the TMO's lattice.[108] $Li(Li_{0.17}Ni_{0.17}Fe_{0.17}Mn_{0.49})O_2$ (Co-free) possessed orphaned oxygen states in the form of Li-O-Li (indicator for CAR[55]). During delithiation, Fe 3d and Ni 3d is first oxidized. Normally, the +3 oxidation state of Fe does not have Jahn-Teller distortion due to the paired e_g orbitals. However, upon oxidation (+3→+4), Jahn-Teller distortion will occur i.e. stretching one of the Fe-O bonds of the FeO_6 octahedron, lowering the energy level of the d_{z2} orbital. This allows for the oxidation of the O(2p) orbital upon further delithiation earlier in the delithiation process (when compared to the non-Fe doped $Li(Li_{0.17}Ni_{0.17}Co_{0.17}Mn_{0.49})O_2$). The authors claimed that the larger amounts of O participating in the redox earlier on in the process produces a lower accumulation of O oxidation in the form of peroxo-like species, which enhances the structural stability of the Fe-doped material.

Li-excess disordered rock salt material (DRX):

Li-excess disordered rock salt material (DRX), have gained significant traction in the recent years. In contrast to the layered materials, rocksalt structures are traditionally considered to be electrochemically inactive due to a lack of percolating Li-ion pathway throughout the bulk structure. This changed when disordered rocksalts were investigated.[21] Work by Cedar *et al*[21,109,110] demonstrated that the $Li_{1.211}Mo_{0.467}Cr_{0.3}O_2$ (LMoCrO) and $Li_{1.25}Nb_{0.25}Mn_{0.5}O_2$ (LNbMO) produce exceptional specific capacities. LMoCrO offered about 265.6 mAh g^{-1} while specific capacities of up to ~300 mAh g^{-1} and 200 mAh g^{-1} were obtained at 50° C and room temperature respectively for LNbMO. LMoCrO was formed as a layered rocksalt structure but developed into a disordered rocksalt upon cycling. **Figure 9a** shows the scanning transmission electron microscopy image of LMoCrO before and after cycling for one and ten cycles. Before cycling, it can be clearly deduced that the structure have more distinct pillars in the Z-contrast line scan (top right of **Figure 9a**). The distinct pillars represent the Li-Mo-Cr ions, with the troughs of these pillars representing Li-ions. After cycling, the Z-contrast decreased with increase in signal from the troughs of the original Li-Mo-Ci pillars (from pristine to 1 and 10 cycles), suggesting the mixing of the cations.

More importantly, the excess Li (particularly above 10%) opened percolating networks of 0-TM, which enhanced the material's Li-ion conductivity. 0-TM Li-ion diffusion mechanism refers to the transport of Li-ions through channels that do not have any TMs at the octahedral sites (in their place Li-ions).[110] Normally in layered material such as $LiCoO_2$, Li-ion transfer occurs through 1-TM channels. However, 1-TM are not suited for Li-ion transport for disordered materials as the size of the tetrahedron are too small due to disordered nature of the structure. In contrast, for disordered materials, 0-TM is the dominating means of Li-ion transport because their migration barrier are lower and should offer more facile transfer of Li-ions.[21] **Figure 9b** plots the simulated 0-TM percolation curve as a function of Li content in the TMO and the degree of cation mixing. The colour red in the contour plot represent a low probability of 0-TM percolation whereas blue represent high. The percolation threshold sits readily from 1.05 to 1.1 at a cation mixing degree of greater than 50%. **Figure 9c** plots the contour plot of electrochemically accessible Li-ions in the disordered rock salt as a function of once again Li content and cation mixing. Interestingly, if the amount of Li in the system does not form a percolating network (when Li content is below 1.05), no Li-ions were calculated to be electrochemically accessible from the disordered rock salt which has been shown experimentally in compounds such as disordered $LiCoO_2$ and $LiNiO_2$.[111]Past this value, the black contour lines labelled as 0.8, 1.0 and 1.2 indicate the amount of accessible Li-ions. This can be seen as the predecessor to the identification of the importance of the Li-O-Li bond.[55] However, this material still exhibited a voltage-fade phenomenon over cycling, similar to the LMR material. Regardless, prior to the discovery of AR in rock salt structures, AR was found only in layered structure. Therefore, the opening of the rock salt materials towards AR offered many new research directions. Rock salt-like structured $Li_4Mn_2O_5$ prepared by a mechanochemical synthesis have been shown to offer exceptional specific capacity (355 mAh g^{-1}).[112] The high capacity was associated with the Mn^{3+}/Mn^{4+}, O^{2-}/O^- and Mn^{4+}/Mn^{5+} but was found to decrease down to ~250 mAh g^{-1} after 8 cycles. The Mn^{4+}/Mn^{5+} redox couple was suggested by magnetic susceptibility studies where the oxidation state of Mn was calculated from the Curie-Weiss fitting of the macroscopic magnetic measurements. Theoretically, the Mn^{3+} to Mn^{4+} redox would only deliver about ~250 mAh g^{-1}.[113]

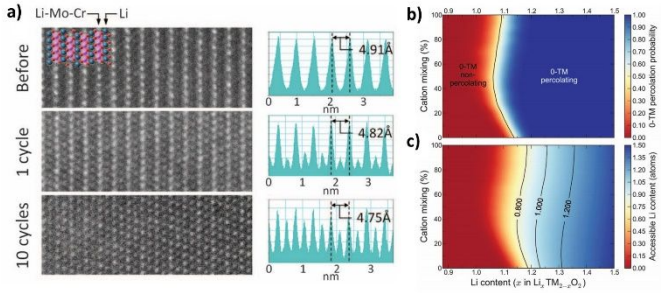

Figure 9: a) Scanning transmission electron microscopy analysis of $Li_{1.211}Mo_{0.467}Cr_{0.3}O_2$ and corresponding intensity plots to the right of sample before cycling, 1st cycle and 10th cycle. b) Li-ion percolation curve and electrochemically accessible Li content as a function of Li content (x in $Li_xTM_{2-x}O_2$) and degree of cation mixing (%). Reproduced with permission. [21] Copyright The American Association for the Advanced of Science 2014.

Li-rich anti-fluorite lithium iron oxide (Li_5FeO_4, LFO) was investigated where simultaneous CAR occurs.[20] The authors demonstrated clear evolution of O_2 and reduction in particle size during the first charge to 4.7 V. The anti-fluorite structure was found to evolve into a disordered rocksalt structure or essentially a DRX material through X-ray diffraction. *In situ* X-ray absorption spectroscopy experiments (**Figure 10a and b** for near-edge and fine structure respectively) revealed a decrease of the Fe-O bond over Stage I (as denoted in **Figure 10c**). Furthermore, the A_1, A_2 and A_3 gradually converted to A_1' and A_2' which is due to the formation of FeO_6 octahedron in the disordered rocksalt phase from the FeO_4 tetrahedron in the pristine LFO material. During the Stage II of the 1st charge process, the F K-edge was found to decrease (Figure 10a), indicating a reduction of the Fe which is likely due to the reduction coupling mechanism as described previously. Interestingly, subsequent cycles were able to remain relatively stable if charged below 3.8 V with relatively minor oxygen release. Overall, it was concluded that the initial charge process of LFO proceeded from an oxidation of Fe^{3+} to Fe^{4+} and O^{2-} to O^- and O_2. During Stage II, the Fe^{4+} is reduced to Fe^{3+} with coupled O^{2-} and O_2 formation, resulting in amorphous $LiFeO_2$ (as shown in **Figure 10d**).[20]

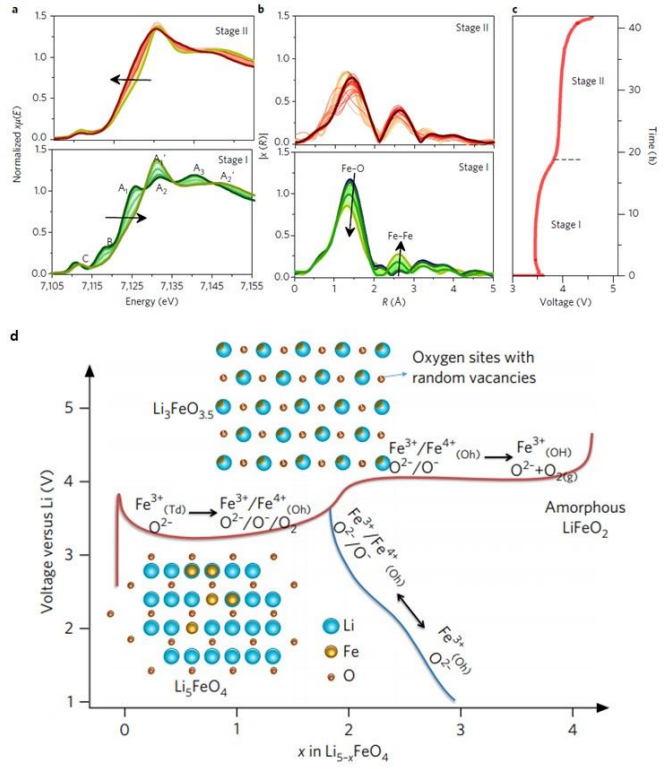

Figure 10: a) In situ X-ray adsorption nears-edge spectroscopy (XANES) and b) extended X-ray fine structure spectroscopy (EXAFS) of Li_5FeO_4 of the Fe K-edge during the first charge to 4.7 V. Corresponding voltage profile shown in c). d) Schematic of the cycling mechanism with regards to the crystal structure and redox centres. Reproduced with permission.[50]Copyright Springer Nature 2017.

Reversible cationic redox:

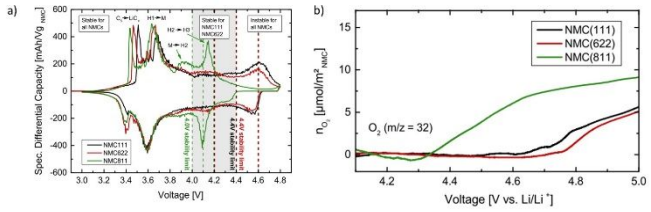

Figure 11: a) Cyclic voltammetry of NMC 111, 622 and 811 full cells up to 4.8 V and b) corresponding O_2 release measured by on-line electrochemical mass spectroscopy. Reproduced with permission.[114] Copyright The Electrochemical Society 2017.

Stable cationic redox based cathodes are widely considered as the leading technological advances towards enabling the LIB. Although the fortunate achievement of a stable SEI is equally if not more important, the inventor of the high performance $LiCoO_2$ (LCO), K. Mizushima and J. Goodenough[115] has been considered to be the father of the LIBs. Originally, LCO is a material that will only achieve reversible cycling with about 50% of its theoretical capacity.[116] Any further increase in charging voltage will lead to irreversible oxygen release as the covalency in the Co-O bond is not high enough to facilitate reversible anion redox. Similarly, contemporary cathode such as the Ni-Mn-Co oxides (NMC) and Ni-Co-Al oxides (NCA) will also undergo similar degradation phenomenon if over-delithiated. Within the stable cycling regime, the redox active component mostly remains to be Co^{3+}/Co^{4+} and the Ni^{2+}/Ni^{4+} double redox[117] with the Mn^{4+} serving mostly as a structural stabilizer.[118] XAS have shown that the capacity of Li-ions extracted from NMC can be accounted for satisfactorily by these two redox centres. [119] Specifically for the NMC class of material, the reversible CR occurs below 4.0 V.[1,120] However, it was well known that at higher charge voltages the system tended to experienced O_2 gas release. This is particularly apparent as the Co content is decreased. Stable cycling voltage decreases from 4.4 V for NMC111 and $LiNi_{0.6}Mn_{0.2}Co_{0.2}O_2$ (NMC622) to 4.0 V for the Ni-rich $LiNi_{0.8}Mn_{0.1}Co_{0.1}O_2$ (NMC811).[114,121] As shown in **Error! Reference source not found.a,** cyclic voltammetry (CV) of NMC 811 exhibited clear oxidation peaks at 4.1 V while the NMC111 and NMC622 compositions remained relatively stable upwards of 4.4 V. On-line electrochemical mass spectroscopy shown in **Error! Reference source not found.b** clearly indicates O_2 release corresponds well to the oxidation peaks observed in the CV. This could be seen a Mott-Hubbard system where the O oxidation occurs very distinctly from CR. In fact, at high enough voltage irreversible O oxidation will occur due to the increase in the covalency of the TM-O bond. However, if the d-band of the TM is well segregated from the 2p of O, there will be a portion of capacity that is exclusively and reversibly CR and is the commonly used regime of capacity for commercial applications.

An interesting case of CR lies in the material Li_3NbO_4, a disordered rocksalt type structure. This material have been shown to offer a high 300 mAh g^{-1} 1st discharge (1.5-4.8 V). [122] While this particular cycling condition did exhibit severe voltage and capacity fade, significant enhancements in stability (both voltage and capacity) was achieved when the cycling was limited to a constant 250 mAh g^{-1} on the charge process. This work associated the capacity and voltage fade with the formation of superoxide-like species upon delithiation. Subsequent further doping of Li_3NbO_4 with Mn, V and Ti yielded significant enhancement in performance.[70] Substitution of Nb for Mn and Fe yielded relatively stable cycling of the O and Mn/Fe redox. However, when V is substituted, forming the composition of $Li_{1.3}Nb_{0.3}V_{0.4}O_2$, the material switched the redox centers from a combined Nb and O to just Nb and V. This was due to the difficulty in the electron transfer (kinetically) from O-ions to the V^{5+}.

More recently and explicitly, Ceder *et al* have demonstrated the concept of increasing the available CR in a TMO as another means of increasing energy density.[123] Transition metal oxyfluorides are compounds that can successfully store Li-ions mostly from CR with a small portion of AR. By using high-valent cations, O^{2-} replacement with F^-, the typically occurring Mn^{4+} is reduced to Mn^{2+}. This allows for the Mn^{2+}/Mn^{4+} double electron redox with a small amount of oxygen redox. As described by Doublet *et al*,[71] this naturally lowers the number of h^o by activating additional cationic redox pairs and effectively increasing the overall reversibility of the cycled anionic redox pair in terms of capacity and voltage fade. In fact, the cycle stability of this material will likely be much more manageable and less inherently limited by O_2 evolution such as the case for many of the typical Li-rich CAR materials. Specifically, $Li_2Mn_{2/3}Nb_{1/3}O_2F$ and $Li_2Mn_{1/2}Ti_{1/2}O_2F$ have a calculated theoretical specific capacity of 270 and 230 respectively based on the Mn^{2+}/Mn^{4+} redox pair. With a minor contribution from O-redox, the obtainable specific capacity of these materials are about 300 mAh g^{-1} (as shown in **Figure 12a**). From Mn K-edge (**Figure 12b**) it was identified that the bonding

environment around Mn changed from MnO-like to Mn_2O_3-like when charged from pristine to 135 mAh g^{-1}. More revealing is the O K-edge (**Figure 12c**), which indicates clear shift towards ~529 eV when the TMO is charged beyond 270 mAh g^{-1}. ~529 eV have been previously associated with MnO_2, suggesting that the Mn in $Li_2Mn_{2/3}Nb_{1/3}O_2F$ did indeed oxidize to +4.[124] Upon discharge to 320 mAh g^{-1}, the O K-edge reverted back to ~531 eV. At the extreme of this spectrum exist the Lithium-rich oxyflourides without any TMs. Li_2VO_2F have been shown to possess over 450 mAh g^{-1} at 2.5 V with only a lattice volume change of 3%.[125] However, this material has no reported anion redox with the capacity of 1.8 Li-ion stemming from only the V^{3+}/V^{5+} redox couple. Interestingly, there was a change in the O K-edge during cycling, which indicates a change in the bonding O bonding environment.

Lastly, it should be noted here that β-Li_2IrO_3 has been recently suggested to not possess true anion redox in the sense that the O adds capacity to the system and not just participates in the redox process of the TM.[73] This was mostly supported by the RIXS measurement which indicated there was no emission at ~522.8 eV (or separate from the 525 eV)s, characteristic of AR.[45] It should be noted that this emission energy is different than the aforementioned 523.7 eV,[27] further indicating the complexity of analysing O RIXS spectrums with the influence of TMs. While many groups previously thought Li_2IrO_3 was an anionic redox material, the large specific capacity is considered by some to be the sole effect of a multi-valent hybridized Ir-O redox, which was ultimately used to reconcile why this material is stable over cycling.[44] As RIXS is likely required to differentiate between the true AR and coupled AR/CR, much work must be placed in revisiting which mechanism is occurring. However, it is important to note that earlier studies of RIXS have detected a similar so-called "fingerprint" feature in O_2 gas.[48]

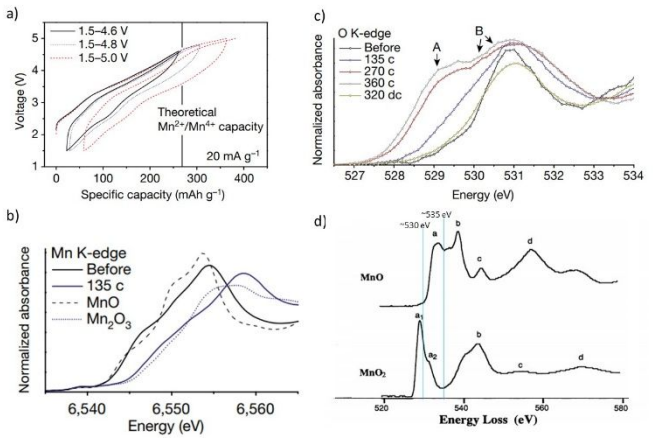

Figure 12: a) First cycle voltage profile of $Li_2Mn_{2/3}Nb_{1/3}O_2F$ with different upper cut-off voltage. b) Mn K-edge and c) O K-edge of $Li_2Mn_{2/3}Nb_{1/3}O_2F$ at different state of charge. Reproduced with permission.[123] Copyright Springer Nature 2018. d) O K-edge of MnO and MnO_2 for comparison. Reproduced with permission.[124] Copyright American Physical Society 2019.

Conclusions

Anionic and cationic redox will continue to hold a significant presence in achieving high energy density Li-ion batteries. Overall, the identification and evidence for CAR revolves around the use of resonant inelastic X-ray scattering. More specifically, AR separate from CR should produce a signal at around an excitation of ~530.9 eV and an emission energy of 522.8 eV,[44]both varying slight among different works,[44,45,64] but all of which are distinct from the broad peak from an emission energy of 522-527 eV across all excitation energies. With the continual development of advanced characterization techniques,[126,127] our understanding and identification of CAR will continue to evolve.

The ability of AR inclusive LIBs to offer increased energy density without significant changes to the cell manufacturing process (changes in electrolyte and anode) makes this type of material highly adoptable and attractive for industry. Many hurdles still exist for CAR before it can be commercialized. Much progress have been made over the past few years regarding the identification of a parameter that can be used to estimate the reversible and extent of anionic redox. From the bond-covalency to the ratio between Li-O and M-O bonds to the recently proposed O hole (h^o), our understanding of reversible CAR has come a long way. The specific definition of anionic redox has been traditionally reserved for O redox that occurs separately from TM redox. In this case, the O redox adds capacity to the system and does not leach capacity from the TM. This type of redox have yet to be shown to be reversible in both capacity and voltage to any sufficient degree. In contrast, β-Li_2IrO_3, which has been shown to be stable due to the redoxing of the hybridized Ir-O and not O and Ir separately,[44] does indeed produce stable cycling with minor voltage hysteresis. Additionally, work into Mn^{2+}/Mn^{4+} double redox[123] (similar to the multivalent Ir redox of β-Li_2IrO_3) have also shown excellent project energy densities with minor voltage fade and good capacity retention. It appears that a system based on a blend of CAR at significant proportions might be not practical while high valent cation redox with a slight addition or capacity boost from AR might be more promising. Finally, the nanolithia mixed with Co_3O_4 might also be a promising direction for future research. Whether this type of material falls in to the definition of AR is up to debate, but it does nevertheless, open new possibilities as a compromise between a full Li-O_2 system and a Li-ion battery.

Conflicts of interest

There are no conflicts to declare

Corresponding Email

junlu@anl.gov (J.L); cheng.zhong@tju.eud.cn (C.Z.)

Acknowledgements

This work is supported by the U. S. Department of Energy (DOE), Office of Energy Efficiency and Renewable Energy, Vehicle Technologies Office. Argonne National Laboratory is operated for DOE Office of Science by UChicago Argonne, LLC, under contract number DE-AC02-06CH11357. C. Zhong acknowledge support from the National Science Foundation for Excellent Young Scholar (No. 51722403), National Natural Science Foundation of China (No. 51771134), the National Natural Science Foundation of China and Guangdong Province

(No. U1601216), and the National Youth Talent Support Program. M. Li would like to acknowledge financial support from the Natural Sciences and Engineering Research Council of Canada (NSERC) and the Waterloo Institute for Nanotechnology (WIN).

Notes and references

(1) Li, M.; Lu, J.; Chen, Z. W.; Amine, K. 30 Years of Lithium-Ion Batteries. *Adv. Mater* **2018**, *30*, 1800561.

(2) Ji, X. L.; Lee, K. T.; Nazar, L. F. A highly ordered nanostructured carbon-sulphur cathode for lithium-sulphur batteries. *Nat. Mater* **2009**, *8*, 500-506.

(3) Li, M.; Zhang, Y.; Hassan, F.; Ahn, W.; Wang, X.; Liu, W. W.; Jiang, G.; Chen, Z. Compact high volumetric and areal capacity lithium sulfur batteries through rock salt induced nano-architectured sulfur hosts. *J. Mater. Chem. A* **2017**, *5*, 21435-21441.

(4) Li, M.; Zhang, Y.; Bai, Z.; Liu, W. W.; Liu, T.; Gim, J.; Jiang, G.; Yuan, Y.; Luo, D.; Feng, K.; Yassar, R. S.; Wang, X.; Chen, Z.; Lu, J. A Lithium–Sulfur Battery using a 2D Current Collector Architecture with a Large-Sized Sulfur Host Operated under High Areal Loading and Low E/S Ratio. *Adv. Mater* **2018**, *30*, 1804271.

(5) Lu, J.; Li, L.; Park, J.-B.; Sun, Y.-K.; Wu, F.; Amine, K. Aprotic and aqueous Li–O2 batteries. *Chem. Rev.* **2014**, *114*, 5611-5640.

(6) Nemori, H.; Shang, X.; Minami, H.; Mitsuoka, S.; Nomura, M.; Sonoki, H.; Morita, Y.; Mori, D.; Takeda, Y.; Yamamoto, O.; Imanishi, N. Aqueous lithium-air batteries with a lithium-ion conducting solid electrolyte $Li_{1.3}Al_{0.5}Nb_{0.2}Ti_{1.3}(PO_4)_3$. *Solid State Ion.* **2018**, *317*, 136-141.

(7) Asadi, M.; Sayahpour, B.; Abbasi, P.; Ngo, A. T.; Karis, K.; Jokisaari, J. R.; Liu, C.; Narayanan, B.; Gerard, M.; Yasaei, P.; Hu, X.; Mukherjee, A.; Lau, K. C.; Assary, R. S.; Khalili-Araghi, F.; Klie, R. F.; Curtiss, L. A.; Salehi-Khojin, A. A lithium-oxygen battery with a long cycle life in an air-like atmosphere. *Nature* **2018**, *555*, 502.

(8) Lu, J.; Jung Lee, Y.; Luo, X.; Chun Lau, K.; Asadi, M.; Wang, H.-H.; Brombosz, S.; Wen, J.; Zhai, D.; Chen, Z.; Miller, D. J.; Sub Jeong, Y.; Park, J.-B.; Zak Fang, Z.; Kumar, B.; Salehi-Khojin, A.; Sun, Y.-K.; Curtiss, L. A.; Amine, K. A lithium–oxygen battery based on lithium superoxide. *Nature* **2016**, *529*, 377.

(9) Fu, J.; Cano, Z. P.; Park, M. G.; Yu, A.; Fowler, M.; Chen, Z. Electrically Rechargeable Zinc–Air Batteries: Progress, Challenges, and Perspectives. *Adv. Mater* **2017**, *29*.

(10) Li, Y.; Dai, H. Recent advances in zinc–air batteries. *Chem. Soc. Rev.* **2014**, *43*, 5257-5275.

(11) Chen, Y.; Ji, S.; Zhao, S.; Chen, W.; Dong, J.; Cheong, W.-C.; Shen, R.; Wen, X.; Zheng, L.; Rykov, A. I.; Cai, S.; Tang, H.; Zhuang, Z.; Chen, C.; Peng, Q.; Wang, D.; Li, Y. Enhanced oxygen reduction with single-atomic-site iron catalysts for a zinc-air battery and hydrogen-air fuel cell. *Nat. Commun* **2018**, *9*, 5422.

(12) Son, S.-B.; Gao, T.; Harvey, S. P.; Steirer, K. X.; Stokes, A.; Norman, A.; Wang, C.; Cresce, A.; Xu, K.; Ban, C. An artificial interphase enables reversible magnesium chemistry in carbonate electrolytes. *Nat. Chem.* **2018**.

(13) Kim, D.-M.; Kim, Y.; Arumugam, D.; Woo, S. W.; Jo, Y. N.; Park, M.-S.; Kim, Y.-J.; Choi, N.-S.; Lee, K. T. Co-intercalation of Mg^{2+} and Na^+ in $Na_{0.69}Fe_2(CN)_6$ as a high-voltage cathode for magnesium batteries. *ACS Appl. Mater. Interfaces* **2016**, *8*, 8554-8560.

(14) Bucur, C. B.; Gregory, T.; Oliver, A. G.; Muldoon, J. Confession of a Magnesium Battery. *J. Phys. Chem. Lett.* **2015**, *6*, 3578-3591.

(15) Tan, Y.-H.; Yao, W.-T.; Zhang, T.; Ma, T.; Lu, L.-L.; Zhou, F.; Yao, H.-B.; Yu, S.-H. High Voltage Magnesium-ion Battery Enabled by Nanocluster Mg_3Bi_2 Alloy Anode in Noncorrosive Electrolyte. *ACS Nano* **2018**, *12*, 5856-5865.

(16) Zhang, J.; Lei, Z.; Wang, J.; NuLi, Y.; Yang, J. Surface Modification of $Li_{1.2}Ni_{0.13}Mn_{0.54}Co_{0.13}O_2$ by Hydrazine Vapor as Cathode Material for Lithium-Ion Batteries. *ACS Appl. Mater. Interfaces* **2015**, *7*, 15821-15829.

(17) Zhang, X.; Belharouak, I.; Li, L.; Lei, Y.; Elam, J. W.; Nie, A.; Chen, X.; Yassar, R. S.; Axelbaum, R. L. Structural and Electrochemical Study of Al_2O_3 and TiO_2 Coated $Li_{1.2}Ni_{0.13}Mn_{0.54}Co_{0.13}O_2$ Cathode Material Using ALD. *Adv. Energy Mater.* **2013**, *3*, 1299-1307.

(18) Karthikeyan, K.; Amaresh, S.; Lee, G. W.; Aravindan, V.; Kim, H.; Kang, K. S.; Kim, W. S.; Lee, Y. S. Electrochemical performance of cobalt free, $Li_{1.2}(Mn_{0.32}Ni_{0.32}Fe_{0.16})O_2$ cathodes for lithium batteries. *Electrochim. Acta* **2012**, *68*, 246-253.

(19) Luo, K.; Roberts, M. R.; Guerrini, N.; Tapia-Ruiz, N.; Hao, R.; Massel, F.; Pickup, D. M.; Ramos, S.; Liu, Y.-S.; Guo, J.; Chadwick, A. V.; Duda, L. C.; Bruce, P. G. Anion Redox Chemistry in the Cobalt Free 3d Transition Metal Oxide Intercalation Electrode Li[Li0.2Ni0.2Mn0.6]O2. *J. Am. Chem. Soc.* **2016**, *138*, 11211-11218.

(20) Saubanere, M.; McCalla, E.; Tarascon, J. M.; Doublet, M. L. The intriguing question of anionic redox in high-energy density cathodes for Li-ion batteries. *Energy Environ. Sci.* **2016**, *9*, 984-991.

(21) Lee, J.; Urban, A.; Li, X.; Su, D.; Hautier, G.; Ceder, G. Unlocking the Potential of Cation-Disordered Oxides for Rechargeable Lithium Batteries. *Science* **2014**, *343*, 519.

(22) Lun, Z.; Ouyang, B.; Kitchaev, D. A.; Clément, R. J.; Papp, J. K.; Balasubramanian, M.; Tian, Y.; Lei, T.; Shi, T.; McCloskey, B. D.; Lee, J.; Ceder, G. Improved Cycling Performance of Li-Excess Cation-Disordered Cathode Materials upon Fluorine Substitution. *Adv. Energy Mater.* **2019**, *9*, 1802959.

(23) Ji, H.; Urban, A.; Kitchaev, D. A.; Kwon, D.-H.; Artrith, N.; Ophus, C.; Huang, W.; Cai, Z.; Shi, T.; Kim, J. C.; Kim, H.; Ceder, G. Hidden structural and chemical order controls lithium transport in cation-disordered oxides for rechargeable batteries. *Nat. Commun* **2019**, *10*, 592.

(24) Assat, G.; Tarascon, J.-M. Fundamental understanding and practical challenges of anionic redox activity in Li-ion batteries. *Nat. Energy* **2018**, 1.

(25) Zhao, C.; Wang, Q.; Lu, Y.; Hu, Y.-S.; Li, B.; Chen, L. Review on anionic redox for high-capacity lithium-and sodium-ion batteries. *Journal of Physics D: Applied Physics* **2017**, *50*, 183001.

(26) Li, B.; Xia, D. Anionic Redox in Rechargeable Lithium Batteries. *Adv. Mater* **2017**, *29*.

(27) Yang, W.; Devereaux, T. P. Anionic and cationic redox and interfaces in batteries: Advances from soft X-ray absorption spectroscopy to resonant inelastic scattering. *J. Power Sources* **2018**, *389*, 188-197.

(28) Hu, E.; Yu, X.; Lin, R.; Bi, X.; Lu, J.; Bak, S.; Nam, K.-W.; Xin, H. L.; Jaye, C.; Fischer, D. A.; Amine, K.; Yang, X.-Q. Evolution of redox couples in Li- and Mn-rich cathode materials and mitigation of voltage fade by reducing oxygen release. *Nat. Energy* **2018**, *3*, 690-698.

(29) Zhu, Z.; Kushima, A.; Yin, Z.; Qi, L.; Amine, K.; Lu, J.; Li, J. Anion-redox nanolithia cathodes for Li-ion batteries. *Nat. Energy* **2016**, *1*, 16111.

(30) Amatucci, G. G. Investigations of the structure, electrochemistry, and processing of the layered lithium cobalt dioxide lithium intercalation host material. Rutgers The State University of New Jersey - New Brunswick, 1997.

(31) Tarascon, J. M.; Vaughan, G.; Chabre, Y.; Seguin, L.; Anne, M.; Strobel, P.; Amatucci, G. In Situ Structural and Electrochemical Study of $Ni_{1-x}Co_xO_2$ Metastable Oxides Prepared by Soft Chemistry. *J. Solid State Chem.* **1999**, *147*, 410-420.

(32) McCalla, E.; Abakumov, A. M.; Saubanère, M.; Foix, D.; Berg, E. J.; Rousse, G.; Doublet, M.-L.; Gonbeau, D.; Novák, P.; Van

Tendeloo, G.; Dominko, R.; Tarascon, J.-M. Visualization of O-O peroxo-like dimers in high-capacity layered oxides for Li-ion batteries. *Science* **2015**, *350*, 1516.

(33) Rouxel, J.: Design and Chemical Reactivity of Low-Dimensional Solids. In *Supramolecular Architecture*; ACS Symposium Series 499; American Chemical Society, 1992; Vol. 499; pp 88-113.

(34) Rouxel, J. Anion–Cation Redox Competition and the Formation of New Compounds in Highly Covalent Systems. *Chem.: Eur. J.* **1996**, *2*, 1053-1059.

(35) Ceder, G.; Chiang, Y. M.; Sadoway, D. R.; Aydinol, M. K.; Jang, Y. I.; Huang, B. Identification of cathode materials for lithium batteries guided by first-principles calculations. *Nature* **1998**, *392*, 694-696.

(36) Sathiya, M.; Rousse, G.; Ramesha, K.; Laisa, C. P.; Vezin, H.; Sougrati, M. T.; Doublet, M. L.; Foix, D.; Gonbeau, D.; Walker, W.; Prakash, A. S.; Ben Hassine, M.; Dupont, L.; Tarascon, J. M. Reversible anionic redox chemistry in high-capacity layered-oxide electrodes. *Nat. Mater* **2013**, *12*, 827.

(37) Yoon, W.-S.; Kim, K.-B.; Kim, M.-G.; Lee, M.-K.; Shin, H.-J.; Lee, J.-M.; Lee, J.-S.; Yo, C.-H. Oxygen Contribution on Li-Ion Intercalation−Deintercalation in $LiCoO_2$ Investigated by O K-Edge and Co L-Edge X-ray Absorption Spectroscopy. *J. Phys. Chem. B* **2002**, *106*, 2526-2532.

(38) Löble, M. W.; Keith, J. M.; Altman, A. B.; Stieber, S. C. E.; Batista, E. R.; Boland, K. S.; Conradson, S. D.; Clark, D. L.; Lezama Pacheco, J.; Kozimor, S. A.; Martin, R. L.; Minasian, S. G.; Olson, A. C.; Scott, B. L.; Shuh, D. K.; Tyliszczak, T.; Wilkerson, M. P.; Zehnder, R. A. Covalency in Lanthanides. An X-ray Absorption Spectroscopy and Density Functional Theory Study of $LnCl_6^{x-}$ (x = 3, 2). *J. Am. Chem. Soc.* **2015**, *137*, 2506-2523.

(39) Solomon, E. I.; Hedman, B.; Hodgson, K. O.; Dey, A.; Szilagyi, R. K. Ligand K-edge X-ray absorption spectroscopy: covalency of ligand–metal bonds. *Coordination Chemistry Reviews* **2005**, *249*, 97-129.

(40) Mizokawa, T.; Wakisaka, Y.; Sudayama, T.; Iwai, C.; Miyoshi, K.; Takeuchi, J.; Wadati, H.; Hawthorn, D. G.; Regier, T. Z.; Sawatzky, G. A. Role of Oxygen Holes in Li_xCoO_2 Revealed by Soft X-Ray Spectroscopy. *Physical Review Letters* **2013**, *111*, 056404.

(41) Liu, X.; Wang, Y. J.; Barbiellini, B.; Hafiz, H.; Basak, S.; Liu, J.; Richardson, T.; Shu, G.; Chou, F.; Weng, T.-C.; Nordlund, D.; Sokaras, D.; Moritz, B.; Devereaux, T. P.; Qiao, R.; Chuang, Y.-D.; Bansil, A.; Hussain, Z.; Yang, W. Why $LiFePO_4$ is a safe battery electrode: Coulomb repulsion induced electron-state reshuffling upon lithiation. *Phys. Chem. Chem. Phys.* **2015**, *17*, 26369-26377.

(42) Qiao, R.; Wray, L. A.; Kim, J.-H.; Pieczonka, N. P. W.; Harris, S. J.; Yang, W. Direct Experimental Probe of the Ni(II)/Ni(III)/Ni(IV) Redox Evolution in $LiNi_{0.5}Mn_{1.5}O_4$ Electrodes. *J. Phys. Chem. C* **2015**, *119*, 27228-27233.

(43) de Groot, F. M. F.; Grioni, M.; Fuggle, J. C.; Ghijsen, J.; Sawatzky, G. A.; Petersen, H. Oxygen 1s x-ray-absorption edges of transition-metal oxides. *Phys. Rev. B* **1989**, *40*, 5715-5723.

(44) Hong, J.; Gent, W. E.; Xiao, P.; Lim, K.; Seo, D.-H.; Wu, J.; Csernica, P. M.; Takacs, C. J.; Nordlund, D.; Sun, C.-J.; Stone, K. H.; Passarello, D.; Yang, W.; Prendergast, D.; Ceder, G.; Toney, M. F.; Chueh, W. C. Metal–oxygen decoordination stabilizes anion redox in Li-rich oxides. *Nat. Mater* **2019**, *18*, 256-265.

(45) Xu, J.; Sun, M.; Qiao, R.; Renfrew, S. E.; Ma, L.; Wu, T.; Hwang, S.; Nordlund, D.; Su, D.; Amine, K.; Lu, J.; McCloskey, B. D.; Yang, W.; Tong, W. Elucidating anionic oxygen activity in lithium-rich layered oxides. *Nat. Commun* **2018**, *9*, 947.

(46) Dai, K.; Wu, J.; Zhuo, Z.; Li, Q.; Sallis, S.; Mao, J.; Ai, G.; Sun, C.; Li, Z.; Gent, W. E.; Chueh, W. C.; Chuang, Y.-d.; Zeng, R.; Shen, Z.-x.; Pan, F.; Yan, S.; Piper, L. F. J.; Hussain, Z.; Liu, G.; Yang, W. High Reversibility of Lattice Oxygen Redox Quantified by Direct Bulk Probes of Both Anionic and Cationic Redox Reactions. *Joule* **2019**, *3*, 518-541.

(47) Zhuo, Z.; Pemmaraju, C. D.; Vinson, J.; Jia, C.; Moritz, B.; Lee, I.; Sallies, S.; Li, Q.; Wu, J.; Dai, K.; Chuang, Y.-d.; Hussain, Z.; Pan, F.; Devereaux, T. P.; Yang, W. Spectroscopic Signature of Oxidized Oxygen States in Peroxides. *J. Phys. Chem. Lett.* **2018**, *9*, 6378-6384.

(48) Glans, P.; Gunnelin, K.; Skytt, P.; Guo, J. H.; Wassdahl, N.; Nordgren, J.; Ågren, H.; Gel'mukhanov, F. K.; Warwick, T.; Rotenberg, E. Resonant X-Ray Emission Spectroscopy of Molecular Oxygen. *Physical Review Letters* **1996**, *76*, 2448-2451.

(49) Assat, G.; Foix, D.; Delacourt, C.; Iadecola, A.; Dedryvère, R.; Tarascon, J.-M. Fundamental interplay between anionic/cationic redox governing the kinetics and thermodynamics of lithium-rich cathodes. *Nat. Commun* **2017**, *8*, 2219.

(50) Zhan, C.; Yao, Z.; Lu, J.; Ma, L.; Maroni, V. A.; Li, L.; Lee, E.; Alp, E. E.; Wu, T.; Wen, J.; Ren, Y.; Johnson, C.; Thackeray, M. M.; Chan, M. K. Y.; Wolverton, C.; Amine, K. Enabling the high capacity of lithium-rich anti-fluorite lithium iron oxide by simultaneous anionic and cationic redox. *Nat. Energy* **2017**, *2*, 963-971.

(51) Zheng, J.; Teng, G.; Yang, J.; Xu, M.; Yao, Q.; Zhuo, Z.; Yang, W.; Liu, Q.; Pan, F. Mechanism of Exact Transition between Cationic and Anionic Redox Activities in Cathode Material Li_2FeSiO_4. *J. Phys. Chem. Lett.* **2018**, *9*, 6262-6268.

(52) McCalla, E.; Sougrati, M. T.; Rousse, G.; Berg, E. J.; Abakumov, A.; Recham, N.; Ramesha, K.; Sathiya, M.; Dominko, R.; Van Tendeloo, G.; Novák, P.; Tarascon, J.-M. Understanding the Roles of Anionic Redox and Oxygen Release during Electrochemical Cycling of Lithium-Rich Layered Li4FeSbO6. *J. Am. Chem. Soc.* **2015**, *137*, 4804-4814.

(53) Kalyani, P.; Chitra, S.; Mohan, T.; Gopukumar, S. Lithium metal rechargeable cells using Li_2MnO_3 as the positive electrode. *J. Power Sources* **1999**, *80*, 103-106.

(54) Thackeray, M. M.; Kang, S.-H.; Johnson, C. S.; Vaughey, J. T.; Benedek, R.; Hackney, S. A. Li2MnO3-stabilized LiMO2 (M = Mn, Ni, Co) electrodes for lithium-ion batteries. *J. Mater. Chem.* **2007**, *17*, 3112-3125.

(55) Seo, D.-H.; Lee, J.; Urban, A.; Malik, R.; Kang, S.; Ceder, G. The structural and chemical origin of the oxygen redox activity in layered and cation-disordered Li-excess cathode materials. *Nat. Chem.* **2016**, *8*, 692.

(56) Hy, S.; Cheng, J.-H.; Liu, J.-Y.; Pan, C.-J.; Rick, J.; Lee, J.-F.; Chen, J.-M.; Hwang, B. J. Understanding the Role of Ni in Stabilizing the Lithium-Rich High-Capacity Cathode Material $Li[Ni^xLi_{(1-2x)/3}Mn_{(2-x)/3}]O_2$ ($0 \le x \le 0.5$). *Chem. Mater.* **2014**, *26*, 6919-6927.

(57) Asadi, M.; Sayahpour, B.; Abbasi, P.; Ngo, A. T.; Karis, K.; Jokisaari, J. R.; Liu, C.; Narayanan, B.; Gerard, M.; Yasaei, P.; Hu, X.; Mukherjee, A.; Lau, K. C.; Assary, R. S.; Khalili-Araghi, F.; Klie, R. F.; Curtiss, L. A.; Salehi-Khojin, A. A lithium–oxygen battery with a long cycle life in an air-like atmosphere. *Nature* **2018**, *555*, 502.

(58) Luo, K.; Roberts, M. R.; Hao, R.; Guerrini, N.; Pickup, D. M.; Liu, Y.-S.; Edström, K.; Guo, J.; Chadwick, A. V.; Duda, L. C.; Bruce, P. G. Charge-compensation in 3d-transition-metal-oxide intercalation cathodes through the generation of localized electron holes on oxygen. *Nat. Chem.* **2016**, *8*, 684.

(59) Mohanty, D.; Sefat, A. S.; Kalnaus, S.; Li, J.; Meisner, R. A.; Payzant, E. A.; Abraham, D. P.; Wood, D. L.; Daniel, C. Investigating phase transformation in the $Li_{1.2}Co_{0.1}Mn_{0.55}Ni_{0.15}O_2$ lithium-ion battery cathode during high-voltage hold (4.5 V) via magnetic, X-ray diffraction and electron microscopy studies. *J. Mater. Chem. A* **2013**, *1*, 6249-6261.

(60) Sathiya, M.; Abakumov, A. M.; Foix, D.; Rousse, G.; Ramesha, K.; Saubanère, M.; Doublet, M. L.; Vezin, H.; Laisa, C. P.;

Prakash, A. S.; Gonbeau, D.; VanTendeloo, G.; Tarascon, J. M. Origin of voltage decay in high-capacity layered oxide electrodes. *Nat. Mater* **2014**, *14*, 230.

(61) Mohanty, D.; Huq, A.; Payzant, E. A.; Sefat, A. S.; Li, J.; Abraham, D. P.; Wood, D. L.; Daniel, C. Neutron Diffraction and Magnetic Susceptibility Studies on a High-Voltage $Li_{1.2}Mn_{0.55}Ni_{0.15}Co_{0.10}O_2$ Lithium Ion Battery Cathode: Insight into the Crystal Structure. *Chem. Mater.* **2013**, *25*, 4064-4070.

(62) Ishida, N.; Tamura, N.; Kitamura, N.; Idemoto, Y. Crystal and electronic structure analysis and thermodynamic stabilities for electrochemically or chemically delithiated $Li_{1.2-x}Mn_{0.54}Ni_{0.13}Co_{0.13}O_2$. *J. Power Sources* **2016**, *319*, 255-261.

(63) Fell, C. R.; Qian, D.; Carroll, K. J.; Chi, M.; Jones, J. L.; Meng, Y. S. Correlation Between Oxygen Vacancy, Microstrain, and Cation Distribution in Lithium-Excess Layered Oxides During the First Electrochemical Cycle. *Chem. Mater.* **2013**, *25*, 1621-1629.

(64) Gent, W. E.; Lim, K.; Liang, Y.; Li, Q.; Barnes, T.; Ahn, S.-J.; Stone, K. H.; McIntire, M.; Hong, J.; Song, J. H.; Li, Y.; Mehta, A.; Ermon, S.; Tyliszczak, T.; Kilcoyne, D.; Vine, D.; Park, J.-H.; Doo, S.-K.; Toney, M. F.; Yang, W.; Prendergast, D.; Chueh, W. C. Coupling between oxygen redox and cation migration explains unusual electrochemistry in lithium-rich layered oxides. *Nat. Commun* **2017**, *8*, 2091.

(65) Grimaud, A.; Hong, W. T.; Shao-Horn, Y.; Tarascon, J. M. Anionic redox processes for electrochemical devices. *Nat. Mater* **2016**, *15*, 121.

(66) Blandeau, L.; Ouvrard, G.; Calage, Y.; Brec, R.; Rouxel, J. Transition-metal dichalcogenides from disintercalation processes. Crystal structure determination and Mossbauer study of Li_2FeS_2 and its disintercalates Li_xFeS_2 ($0.2 \leq x \leq 2$). *Journal of Physics C: Solid State Physics* **1987**, *20*, 4271.

(67) Li, B.; Jiang, N.; Huang, W.; Yan, H.; Zuo, Y.; Xia, D. Thermodynamic Activation of Charge Transfer in Anionic Redox Process for Li-Ion Batteries. *Adv. Funct. Mater.* **2018**, *28*, 1704864.

(68) Xie, Y.; Saubanere, M.; Doublet, M. L. Requirements for reversible extra-capacity in Li-rich layered oxides for Li-ion batteries. *Energy Environ. Sci.* **2017**, *10*, 266-274.

(69) Zaanen, J.; Sawatzky, G. A.; Allen, J. W. Band gaps and electronic structure of transition-metal compounds. *Physical Review Letters* **1985**, *55*, 418-421.

(70) Yabuuchi, N.; Nakayama, M.; Takeuchi, M.; Komaba, S.; Hashimoto, Y.; Mukai, T.; Shiiba, H.; Sato, K.; Kobayashi, Y.; Nakao, A.; Yonemura, M.; Yamanaka, K.; Mitsuhara, K.; Ohta, T. Origin of stabilization and destabilization in solid-state redox reaction of oxide ions for lithium-ion batteries. *Nat. Commun* **2016**, *7*, 13814.

(71) Ben Yahia, M.; Vergnet, J.; Saubanère, M.; Doublet, M.-L. Unified picture of anionic redox in Li/Na-ion batteries. *Nat. Mater* **2019**, *18*, 496-502.

(72) Seo, D.-H.; Urban, A.; Ceder, G. Calibrating transition-metal energy levels and oxygen bands in first-principles calculations: Accurate prediction of redox potentials and charge transfer in lithium transition-metal oxides. *Phys. Rev. B* **2015**, *92*, 115118.

(73) Pearce, P. E.; Perez, A. J.; Rousse, G.; Saubanère, M.; Batuk, D.; Foix, D.; McCalla, E.; Abakumov, A. M.; Van Tendeloo, G.; Doublet, M.-L.; Tarascon, J.-M. Evidence for anionic redox activity in a tridimensional-ordered Li-rich positive electrode β-Li_2IrO_3. *Nat. Mater* **2017**, *16*, 580.

(74) Yabuuchi, N. Material Design Concept of Lithium-Excess Electrode Materials with Rocksalt-Related Structures for Rechargeable Non-Aqueous Batteries. *The Chemical Record* **2019**, *19*, 690-707.

(75) Sathiya, M.; Ramesha, K.; Rousse, G.; Foix, D.; Gonbeau, D.; Prakash, A. S.; Doublet, M. L.; Hemalatha, K.; Tarascon, J. M. High Performance $Li_2Ru_{1-y}Mn_yO_3$ ($0.2 \leq y \leq 0.8$) Cathode Materials for Rechargeable Lithium-Ion Batteries: Their Understanding. *Chem. Mater.* **2013**, *25*, 1121-1131.

(76) Zhang, L.; Sun, D.; Feng, J.; Cairns, E. J.; Guo, J. Revealing the Electrochemical Charging Mechanism of Nanosized Li2S by in Situ and Operando X-ray Absorption Spectroscopy. *Nano Lett.* **2017**, *17*, 5084-5091.

(77) Li, M.; Chen, Z.; Wu, T.; Lu, J. Li_2S- or S-Based Lithium-Ion Batteries. *Adv. Mater* **2018**, *30*, 1801190.

(78) Lu, J.; Lei, Y.; Lau, K. C.; Luo, X.; Du, P.; Wen, J.; Assary, R. S.; Das, U.; Miller, D. J.; Elam, J. W.; Albishri, H. M.; El-Hady, D. A.; Sun, Y.-K.; Curtiss, L. A.; Amine, K. A nanostructured cathode architecture for low charge overpotential in lithium-oxygen batteries. *Nat. Commun* **2013**, *4*, 2383.

(79) Okuoka, S.-i.; Ogasawara, Y.; Suga, Y.; Hibino, M.; Kudo, T.; Ono, H.; Yonehara, K.; Sumida, Y.; Yamada, Y.; Yamada, A.; Oshima, M.; Tochigi, E.; Shibata, N.; Ikuhara, Y.; Mizuno, N. A New Sealed Lithium-Peroxide Battery with a Co-Doped Li_2O Cathode in a Superconcentrated Lithium Bis(fluorosulfonyl)amide Electrolyte. *Sci. Rep.* **2014**, *4*, 5684.

(80) Qiao, Y.; Jiang, K.; Deng, H.; Zhou, H. A high-energy-density and long-life lithium-ion battery via reversible oxide–peroxide conversion. *Nature Catalysis* **2019**.

(81) Li, M.; Bai, Z.; Li, Y.; Ma, L.; Dai, A.; Wang, X.; Luo, D.; Wu, T.; Liu, P.; Yang, L.; Amine, K.; Chen, Z.; Lu, J. Electrochemically primed functional redox mediator generator from the decomposition of solid state electrolyte. *Nat. Commun* **2019**, *10*, 1890.

(82) Yang, Y.; Zheng, G.; Misra, S.; Nelson, J.; Toney, M. F.; Cui, Y. High-Capacity Micrometer-Sized Li2S Particles as Cathode Materials for Advanced Rechargeable Lithium-Ion Batteries. *J. Am. Chem. Soc.* **2012**, *134*, 15387-15394.

(83) Gorlin, Y.; Patel, M. U. M.; Freiberg, A.; He, Q.; Piana, M.; Tromp, M.; Gasteiger, H. A. Understanding the Charging Mechanism of Lithium-Sulfur Batteries Using Spatially Resolved Operando X-Ray Absorption Spectroscopy. *J. Electrochem. Soc.* **2016**, *163*, A930-A939.

(84) Tan, G.; Xu, R.; Xing, Z.; Yuan, Y.; Lu, J.; Wen, J.; Liu, C.; Ma, L.; Zhan, C.; Liu, Q.; Wu, T.; Jian, Z.; Shahbazian-Yassar, R.; Ren, Y.; Miller, D. J.; Curtiss, L. A.; Ji, X.; Amine, K. Burning lithium in CS_2 for high-performing compact Li_2S–graphene nanocapsules for Li–S batteries. *Nat. Energy* **2017**, *2*, 17090.

(85) Liu, Z.; Deng, H.; Hu, W.; Gao, F.; Zhang, S.; Balbuena, P. B.; Mukherjee, P. P. Revealing Reaction Mechanisms of Nanoconfined Li2S: Implications for Lithium-Sulfur Batteries. *Phys. Chem. Chem. Phys.* **2018**.

(86) Meng, X.; Comstock, D. J.; Fister, T. T.; Elam, J. W. Vapor-phase atomic-controllable growth of amorphous Li2S for high-performance lithium–sulfur batteries. *ACS Nano* **2014**, *8*, 10963-10972.

(87) Lu, Z.; MacNeil, D. D.; Dahn, J. R. Layered Cathode Materials $Li[Ni_x Li_{(1/3-2x/3)} Mn_{(2/3-x/3)}]O_2$ for Lithium-Ion Batteries. *Electrochem. Solid-State Lett.* **2001**, *4*, A191-A194.

(88) Lu, Z.; Dahn, J. R. Understanding the Anomalous Capacity of $Li/Li[Ni_x Li_{(1/3-2x/3)} Mn_{(2/3-x/3)}]O_2$ Cells Using In Situ X-Ray Diffraction and Electrochemical Studies. *J. Electrochem. Soc.* **2002**, *149*, A815-A822.

(89) Gummow, R. J.; de Kock, A.; Thackeray, M. M. Improved capacity retention in rechargeable 4 V lithium/lithium-manganese oxide (spinel) cells. *Solid State Ion.* **1994**, *69*, 59-67.

(90) Nayak, P. K.; Erickson, E. M.; Schipper, F.; Penki, T. R.; Munichandraiah, N.; Adelhelm, P.; Sclar, H.; Amalraj, F.; Markovsky, B.; Aurbach, D. Review on Challenges and Recent Advances in the Electrochemical Performance of High Capacity Li- and Mn-Rich Cathode Materials for Li-Ion Batteries. *Adv. Energy Mater.* **2018**, *8*, 1702397.

(91) Rozier, P.; Tarascon, J. M. Review—Li-Rich Layered

Oxide Cathodes for Next-Generation Li-Ion Batteries: Chances and Challenges. *J. Electrochem. Soc.* **2015**, *162*, A2490-A2499.

(92) Lin, J.; Mu, D.; Jin, Y.; Wu, B.; Ma, Y.; Wu, F. Li-rich layered composite $Li[Li_{0.2}Ni_{0.2}Mn_{0.6}]O_2$ synthesized by a novel approach as cathode material for lithium ion battery. *J. Power Sources* **2013**, *230*, 76-80.

(93) Zeng, X.; Li, M.; Abd El-Hady, D.; Alshitari, W.; Al-Bogami, A. S.; Lu, J.; Amine, K. Commercialization of Lithium Battery Technologies for Electric Vehicles. *Adv. Energy Mater.* **2019**, *9*, 1900161.

(94) Lin, F.; Markus, I. M.; Nordlund, D.; Weng, T.-C.; Asta, M. D.; Xin, H. L.; Doeff, M. M. Surface reconstruction and chemical evolution of stoichiometric layered cathode materials for lithium-ion batteries. *Nat. Commun* **2014**, *5*, 3529.

(95) Zheng, J.; Gu, M.; Xiao, J.; Polzin, B. J.; Yan, P.; Chen, X.; Wang, C.; Zhang, J.-G. Functioning Mechanism of AlF_3 Coating on the Li- and Mn-Rich Cathode Materials. *Chem. Mater.* **2014**, *26*, 6320-6327.

(96) Zheng, J.; Gu, M.; Xiao, J.; Zuo, P.; Wang, C.; Zhang, J.-G. Corrosion/Fragmentation of Layered Composite Cathode and Related Capacity/Voltage Fading during Cycling Process. *Nano Lett.* **2013**, *13*, 3824-3830.

(97) Shi, S. J.; Tu, J. P.; Tang, Y. Y.; Liu, X. Y.; Zhang, Y. Q.; Wang, X. L.; Gu, C. D. Enhanced cycling stability of $Li[Li_{0.2}Mn_{0.54}Ni_{0.13}Co_{0.13}]O_2$ by surface modification of MgO with melting impregnation method. *Electrochim. Acta* **2013**, *88*, 671-679.

(98) Liu, J.; Manthiram, A. Functional surface modifications of a high capacity layered $Li[Li_{0.2}Mn_{0.54}Ni_{0.13}Co_{0.13}]O_2$ cathode. *J. Mater. Chem.* **2010**, *20*, 3961-3967.

(99) West, W. C.; Soler, J.; Smart, M. C.; Ratnakumar, B. V.; Firdosy, S.; Ravi, V.; Anderson, M. S.; Hrbacek, J.; Lee, E. S.; Manthiram, A. Electrochemical Behavior of Layered Solid Solution Li_2MnO_3−$LiMO_2$ (M = Ni, Mn, Co) Li-Ion Cathodes with and without Alumina Coatings. *J. Electrochem. Soc.* **2011**, *158*, A883-A889.

(100) Wu, F.; Zhang, X.; Zhao, T.; Li, L.; Xie, M.; Chen, R. Multifunctional AlPO4 Coating for Improving Electrochemical Properties of Low-Cost $Li[Li_{0.2}Fe_{0.1}Ni_{0.15}Mn_{0.55}]O_2$ Cathode Materials for Lithium-Ion Batteries. *ACS Appl. Mater. Interfaces* **2015**, *7*, 3773-3781.

(101) Lee, J.; Choi, W. Surface Modification of Over-Lithiated Layered Oxides with PEDOT:PSS Conducting Polymer in Lithium-Ion Batteries. *J. Electrochem. Soc.* **2015**, *162*, A743-A748.

(102) Nayak, P. K.; Grinblat, J.; Levi, M.; Levi, E.; Kim, S.; Choi, J. W.; Aurbach, D. Al Doping for Mitigating the Capacity Fading and Voltage Decay of Layered Li and Mn-Rich Cathodes for Li-Ion Batteries. *Adv. Energy Mater.* **2016**, *6*.

(103) Qing, R.-P.; Shi, J.-L.; Xiao, D.-D.; Zhang, X.-D.; Yin, Y.-X.; Zhai, Y.-B.; Gu, L.; Guo, Y.-G. Enhancing the Kinetics of Li-Rich Cathode Materials through the Pinning Effects of Gradient Surface Na^+ Doping. *Adv. Energy Mater.* **2016**, *6*, 1501914.

(104) Liu, W.; Oh, P.; Liu, X.; Lee, M.-J.; Cho, W.; Chae, S.; Kim, Y.; Cho, J. Nickel-Rich Layered Lithium Transition-Metal Oxide for High-Energy Lithium-Ion Batteries. *Angew. Chem. Int. Ed* **2015**, *54*, 4440-4457.

(105) Park, S. H.; Shin, S. S.; Sun, Y. K. The effects of Na doping on performance of layered $Li_{1.1-x}Na_x[Ni_{0.2}Co_{0.3}Mn_{0.4}]O_2$ materials for lithium secondary batteries. *Mater. Chem. Phys.* **2006**, *95*, 218-221.

(106) Rossouw, M. H.; Thackeray, M. M. Lithium manganese oxides from Li_2MnO_3 for rechargeable lithium battery applications. *Mater. Res. Bull.* **1991**, *26*, 463-473.

(107) Kobayashi, H.; Tabuchi, M.; Shikano, M.; Kageyama, H.; Kanno, R. Structure, and magnetic and electrochemical properties of layered oxides, Li_2IrO_3. *J. Mater. Chem.* **2003**, *13*, 957-962.

(108) Wei, H.; Cheng, X.; Fan, H.; Shan, Q.; An, S.; Qiu, X.; Jia, G. A Cobalt-Free $Li(Li_{0.17}Ni_{0.17}Fe_{0.17}Mn_{0.49})O_2$ Cathode with More Oxygen-Involving Charge Compensation for Lithium-Ion Batteries. *ChemSusChem* **2019**, *12*, 2471-2479.

(109) Wang, R.; Li, X.; Liu, L.; Lee, J.; Seo, D.-H.; Bo, S.-H.; Urban, A.; Ceder, G. A disordered rock-salt Li-excess cathode material with high capacity and substantial oxygen redox activity: $Li_{1.25}Nb_{0.25}Mn_{0.5}O_2$. *Electrochem. Commun.* **2015**, *60*, 70-73.

(110) Urban, A.; Lee, J.; Ceder, G. The Configurational Space of Rocksalt-Type Oxides for High-Capacity Lithium Battery Electrodes. *Adv. Energy Mater.* **2014**, *4*, 1400478.

(111) Obrovac, M. N.; Mao, O.; Dahn, J. R. Structure and electrochemistry of $LiMO_2$ (M=Ti, Mn, Fe, Co, Ni) prepared by mechanochemical synthesis. *Solid State Ion.* **1998**, *112*, 9-19.

(112) Yao, Z.; Kim, S.; He, J.; Hegde, V. I.; Wolverton, C. Interplay of cation and anion redox in $Li_4Mn_2O_5$ cathode material and prediction of improved $Li_4(Mn,M)_2O_5$ electrodes for Li-ion batteries. *Sci. Adv.* **2018**, *4*, eaao6754.

(113) Freire, M.; Kosova, N. V.; Jordy, C.; Chateigner, D.; Lebedev, O. I.; Maignan, A.; Pralong, V. A new active Li–Mn–O compound for high energy density Li-ion batteries. *Nat. Mater* **2015**, *15*, 173.

(114) Jung, R.; Metzger, M.; Maglia, F.; Stinner, C.; Gasteiger, H. A. Oxygen Release and Its Effect on the Cycling Stability of LiNixMnyCozO2 (NMC) Cathode Materials for Li-Ion Batteries. *J. Electrochem. Soc.* **2017**, *164*, A1361-A1377.

(115) Mizushima, K.; Jones, P. C.; Wiseman, P. J.; Goodenough, J. B. LixCoO2 (0<x<-1): A new cathode material for batteries of high energy density. *Mater. Res. Bull.* **1980**, *15*, 783-789.

(116) Reimers, J. N.; Dahn, J. R. Electrochemical and In Situ X-Ray Diffraction Studies of Lithium Intercalation in Li_xCoO_2. *J. Electrochem. Soc.* **1992**, *139*, 2091-2097.

(117) Zhang, X.; Jiang, W. J.; Mauger, A.; Qilu; Gendron, F.; Julien, C. M. Minimization of the cation mixing in Li1+x(NMC)1−xO2 as cathode material. *J. Power Sources* **2010**, *195*, 1292-1301.

(118) Yoon, W.-S.; Grey, C. P.; Balasubramanian, M.; Yang, X.-Q.; Fischer, D. A.; McBreen, J. Combined NMR and XAS Study on Local Environments and Electronic Structures of Electrochemically Li-Ion Deintercalated $Li_{1-x}Co_{1/3}Ni_{1/3}Mn_{1/3}O_2$ Electrode System. *Electrochem. Solid-State Lett.* **2004**, *7*, A53-A55.

(119) Liu, X.; Wang, D.; Liu, G.; Srinivasan, V.; Liu, Z.; Hussain, Z.; Yang, W. Distinct charge dynamics in battery electrodes revealed by in situ and operando soft X-ray spectroscopy. *Nat. Commun* **2013**, *4*, 2568.

(120) Singh, M.; Kaiser, J.; Hahn, H. Thick Electrodes for High Energy Lithium Ion Batteries. *J. Electrochem. Soc.* **2015**, *162*, A1196-A1201.

(121) Jung, R.; Metzger, M.; Maglia, F.; Stinner, C.; Gasteiger, H. A. Chemical versus Electrochemical Electrolyte Oxidation on NMC111, NMC622, NMC811, LNMO, and Conductive Carbon. *J. Phys. Chem. Lett.* **2017**, *8*, 4820-4825.

(122) Yabuuchi, N.; Takeuchi, M.; Nakayama, M.; Shiiba, H.; Ogawa, M.; Nakayama, K.; Ohta, T.; Endo, D.; Ozaki, T.; Inamasu, T.; Sato, K.; Komaba, S. High-capacity electrode materials for rechargeable lithium batteries: Li_3NbO_4-based system with cation-disordered rocksalt structure. *Proc. Natl. Acad. Sci.* **2015**, *112*, 7650.

(123) Lee, J.; Kitchaev, D. A.; Kwon, D.-H.; Lee, C.-W.; Papp, J. K.; Liu, Y.-S.; Lun, Z.; Clément, R. J.; Shi, T.; McCloskey, B. D.; Guo, J.; Balasubramanian, M.; Ceder, G. Reversible Mn^{2+}/Mn^{4+} double redox in lithium-excess cathode materials. *Nature* **2018**, *556*, 185-190.

(124) Kurata, H.; Lefèvre, E.; Colliex, C.; Brydson, R. Electron-energy-loss near-edge structures in the oxygen K-edge spectra of transition-metal oxides. *Phys. Rev. B* **1993**, *47*, 13763-13768.

(125) Chen, R.; Ren, S.; Knapp, M.; Wang, D.; Witter, R.; Fichtner, M.; Hahn, H. Disordered Lithium-Rich Oxyfluoride as a

Stable Host for Enhanced Li^+ Intercalation Storage. *Adv. Energy Mater.* **2015**, *5*, 1401814.

(126) Yuan, Y.; Amine, K.; Lu, J.; Shahbazian-Yassar, R. Understanding materials challenges for rechargeable ion batteries with in situ transmission electron microscopy. *Nat. Commun* **2017**, *8*, 15806.

(127) Lu, J.; Wu, T.; Amine, K. State-of-the-art characterization techniques for advanced lithium-ion batteries. *Nat. Energy* **2017**, *2*, 17011.

Table of contents:

This review will present the current understanding, experimental evidence and future direction of anionic and cationic redox for Li-ion batteries.